



**3D-Localization of an Unmanned Aerial Vehicle Based on  
Combination of Inertial Motion, GPS and Vision Information**

**Thanabadee Bulunseechart**

**A Thesis Submitted in Partial Fulfillment of the Requirements for the  
Degree of Master of Engineering in Mechanical Engineering  
Prince of Songkla University  
2018**

**Copyright of Prince of Songkla University**



**3D-Localization of an Unmanned Aerial Vehicle Based on  
Combination of Inertial Motion, GPS and Vision Information**

**Thanabadee Bulunseechart**

**A Thesis Submitted in Partial Fulfillment of the Requirements for the  
Degree of Master of Engineering in Mechanical Engineering  
Prince of Songkla University  
2018  
Copyright of Prince of Songkla University**

**Thesis Title**            3D-Localization of an Unmanned Aerial Vehicle Based  
on Combination of Inertial Motion, GPS and Vision  
Information

**Author**                    Mr. Thanabadee Bulunseechart

**Major Program**        Mechanical Engineering

---

**Major Advisor**

.....  
(Assoc. Prof. Dr. Pruittikorn Smithmaitrie)

**Examining Committee :**

.....Chairperson  
(Dr. Paramin Neranon)

.....Committee  
(Assoc. Prof. Dr. Pruittikorn Smithmaitrie)

.....Committee  
(Assoc. Prof. Dr. Sutthiphong Srigrarom)

The Graduate School, Prince of Songkla University, has approved this thesis as partial fulfillment of the requirements for the Master of Engineering Degree in Mechanical Engineering

.....  
(Prof. Dr. Damrongsak Faroongsarng)  
Dean of Graduate School

This is to certify that the work here submitted is the result of the candidate's own investigations. Due acknowledgement has been made of any assistance received.

.....Signature  
(Assoc. Prof. Dr. Pruittikorn Smithmaitrie)  
Major Advisor

.....Signature  
(Mr. Thanabadee Bulunseechart)  
Candidate

I hereby certify that this work has not been accepted in substance for any degree, and is not being currently submitted in candidature for any degree.

.....Signature  
(Mr. Thanabadee Bulunseechart)  
Candidate

ชื่อวิทยานิพนธ์	การระบุตำแหน่งในสามมิติของอากาศยานไร้คนขับด้วยการประมวลผลข้อมูลร่วมของการเคลื่อนที่ จีพีเอส และภาพ
ผู้เขียน	นายธนบดี บุหลันศรีชาติ
สาขาวิชา	วิศวกรรมเครื่องกล
ปีการศึกษา	2561

## บทคัดย่อ

อากาศยานไร้คนขับ หรือยูเอวี ได้ถูกพัฒนาขึ้นเพื่อทดแทนการปฏิบัติงานของมนุษย์ในสถานที่ซับซ้อน และเสี่ยงภัย ในหลายๆงานที่จำเป็นต้องปฏิบัติการใกล้บริเวณตึกสูง หรือในบริเวณซึ่งเป็นเหตุให้สัญญาณจีพีเอสถูกรบกวนขาดความต่อเนื่อง หรือไม่สามารระบุตำแหน่งได้ งานวิจัยนี้จึงใช้วิธีผสมข้อมูลจากตัวตรวจวัดหลายชนิดเพื่อประมาณตำแหน่งของยูเอวี

ปัจจัยสำคัญในการประมาณตำแหน่งของยูเอวีที่มีสมการระบบแบบไม่เชิงเส้นได้แก่ ความแม่นยำ การตอบสนองที่รวดเร็ว และใช้การคำนวณน้อย ในส่วนแรกของงานวิจัยได้เปรียบเทียบประสิทธิภาพของซอฟต์แวร์ตัวประมาณสถานะสามชนิด คือ inertial navigation, robot localization และ Ethzasl MSF ทั้งสามระเบียบวิธีทำงานบนระบบปฏิบัติการหุ่นยนต์ (Robot Operating System, ROS) บนยูเอวีลำเดียวกัน การทดสอบบินแบบระยะทางสั้นและยาวใช้ตำแหน่งจากจีพีเอสเป็นค่าอ้างอิง จากนั้นระเบียบวิธีทั้งสามถูกตรวจวัดและเปรียบเทียบในแง่ของ ความแม่นยำ ความเร็วในการประมาณตำแหน่ง และภาระในการคำนวณ ผลการทดลองแสดงให้เห็นว่า Ethzasl MSF มีประสิทธิภาพที่ดีที่สุดในแง่ของความเร็วในการประมาณตำแหน่ง และมีความแม่นยำกับภาระในการคำนวณในเกณฑ์ที่ยอมรับได้ ยิ่งไปกว่านั้นยังง่ายต่อการเพิ่มตัวตรวจวัดเพื่อเพิ่มเติมข้อมูลประมาณตำแหน่งในสภาพแวดล้อมที่ซับซ้อน

ในส่วนที่สอง ระเบียบวิธีสำหรับระบุตำแหน่งในสามมิติในขณะที่มีการเปลี่ยนผ่านสภาพแวดล้อมระหว่างภายในและภายนอกอาคาร ได้ถูกนำเสนอด้วยการใช้ตัวตรวจวัดหลายชนิด ได้แก่ จีพีเอส ตัวตรวจวัดความเฉื่อย (inertial measurement unit) กล้องตาเดี่ยว และ optical flow sensor ซึ่งถูกเลือกใช้จากเงื่อนไขของสภาพแวดล้อมตามการเปลี่ยนแปลงของความแปรปรวนของจีพีเอสโดยใช้ระเบียบวิธี GPS quality indicator จากนั้นระเบียบวิธี smoothing offset ได้ถูก

นำมาใช้เพื่อปรับปรุงค่าการประมาณตำแหน่งให้ต่อเนื่องและมีแนววิถีที่เหมาะสมกับสถานะ ข้อมูลจากตัวตรวจวัดที่ถูกเลือก ถูกกรองโดยใช้ indirect extended Kalman filter เพื่อระบุตำแหน่ง และเปรียบเทียบตัวตรวจวัด ผลการทดลองได้แสดงให้เห็นว่า การระบุตำแหน่งของยูเอวี มีความต่อเนื่องในการปฏิบัติการระหว่างภายในและภายนอกอาคาร ยิ่งไปกว่านั้น ระเบียบวิธีในการคัดเลือกข้อมูลยังสามารถเลือกใช้ข้อมูลจีพีเอสได้รวดเร็วกว่าการระเบียบวิธีการตัดการทำงานจีพีเอสแบบทั่วไป

**Thesis Title** 3D-Localization of an Unmanned Aerial Vehicle Based on Combination of Inertial Motion, GPS and Vision Information.

**Author** Mr. Thanabadee Bulunseechart

**Major Program** Mechanical Engineering

**Academic Year** 2018

### **Abstract**

Unmanned aerial vehicles (UAVs) have been developed to replace human operation in complex and hazardous environments. Continuity of a UAV operation when GPS is degraded or denied is crucial in many applications such as flying near high buildings and trees, or flying outdoor-to-indoor. The state estimation is used to determine the UAV position and other states from the sensors fusion algorithm.

In order to estimate position of an UAV which is a nonlinear dynamic system, accuracy, fast response and less computational burden are important requirements. In the first part, this thesis compares performance of three state estimation algorithms: inertial navigation, robot localization and Ethzasl MSF frameworks. They are implemented on ROS (Robot Operating System) to control the same UAV platform. In the experiment, GPS measurement is referred as absolute ground position for short and long flight dataset. Then, the state estimators are investigated in term of accuracy, speed and computational burden. The experimental results show that Ethzasl MSF framework has outperformed good estimation response, acceptable accuracy and reasonable computational burden. Moreover, its flexibility allows users to add other sensory information for complex scenarios.

In second part, an algorithm for 3D-localization during transition between indoor and outdoor environments for a UAV is presented. Localization inputs are based on information from GPS, inertial measurement unit (IMU), monocular camera and optical flow sensor. The information is carefully selected corresponding to the operating environment regarding the GPS quality indicator which based on GPS



gradient of variance. After that, the proposed smoothing offset approach is employed to smooth the position estimation. The selected sensor data are filtered by indirect extended Kalman filter for localization and extrinsic sensor calibration in real-time. The results show, the proposed smoothing offset generates a seamless and reasonable flight trajectory of UAV for indoor-outdoor transition. Moreover, the method of decision-making to cutoff GPS measurement even when it experiences poor signal quality can still outperform conventional GPS- based cutoff method in terms of response time.

## **Acknowledgment**

I would like to thank my supervisor Asst. Prof. Dr. Pruittikorn Smithmaitrie for his great support and guidance. I would also like to thank all members of committee: Dr. Paramin Neranon, Assoc. Prof. Dr. Pruittikorn Smithmaitrie and Assoc.Prof. Dr. Spot Srigrarom for generously offering their time, support, guidance and good will throughout the preparation and review of this thesis.

I would like to thank the smart mechatronics research laboratory for financial support and Intel Cooperation (Thailand) for provision of an Intel NUC computer. I would like to thank Mr.Wiwat Sutiwipakorn for his writing review and meaningful advice.

I am thankful to my friends and my parents for their support and encouragement throughout the years.

Thanabadee Bulunseechart

## Contents

	<b>Page</b>
บทคัดย่อ	v
Abstract	vii
Acknowledgment	ix
Contents	x
List of Figures	xii
List of Abbreviations and Symbols	xiv
List of Publications	xviii
Reprint were made with permission from publisher	xix
Introduction	1
<b>Publication of conference paper:</b> Comparison of state estimation algorithms for autonomous GPS-inertial navigation for UAV application	6
1. Introduction	7
2. State estimation algorithms	7
2.1. The inertial navigation (INAV)	8
2.2. The robot localization (RL)	8
2.3. The modified MSF framework (MSF)	9
3. Experimental setup	10
4. Results	11
5. Conclusion	12
References	12
<b>Publication of journal article:</b> A Method for UAV Multi-Sensor Fusion 3D-Localization under Degraded or Denied GPS Situation.	23
1. Introduction	25
2. Multi-sensor fusion	26

2.1 Indirect extended Kalman filter	26
2.2 Measurement of sensors	27
2.2.1. GPS measurement	27
2.2.2. Vision measurement	29
2.2.3. Barometer measurement	30
2.2.4. Optical flow measurement	31
2.2.5. Terrain measurement	31
3. GPS quality indicator	32
4. Pre-scale process in vision measurement	33
5. Seamless transition position measurement	35
6. Implementation and setup	37
6.1. The UAV platform	37
6.2. Real-time onboard software	37
6.3. Control system	37
6.4. Determination of system parameters	37
7. Experimental results	39
8. Conclusion	44
9. Acknowledgments	44
References	44

## List of Figures

	<b>Page</b>
 <b>Chapter 2: Comparison of state estimation algorithms for autonomous GPS-inertial navigation for UAV application</b>	
Figure. 1. The INAV algorithm used in PX4 firmware.	8
Figure. 2. Sensor measurement and state variables of the robot localization package	9
Figure. 3. The tested quadrotor UAV.	10
Figure. 4. Position estimation results of short flight testing.	11
Figure. 5. Position estimation results of long flight testing in large scale view.	11
Figure. 6. Position estimation (x-direction) and error compared with ground truth of the short flight test.	11
Figure. 7. Position estimation (x-direction) and error compared with ground truth of the long flight test.	11
 <b>Chapter 3: A Method for UAV Multi-Sensor Fusion 3D-Localization under Degraded or Denied GPS Situation</b>	
Figure. 1. The UAV reference frames.	27
Figure. 2. The Indirect extended Kalman filter flowchart.	28
Figure. 3. The vision measurement algorithm flowchart.	30
Figure. 4. Relationship between terrain height, above-ground level (AGL) and estimated UAV altitude from the barometer.	32
Figure. 5. Criteria function for increasing GPS variance and decreasing GPS variance.	34
Figure. 6. Estimated position behavior from different GPS position measurement and vision position measurement	36
Figure. 7. The tested UAV setup.	37

Figure. 8	Processing workflow diagram of the UAV system.	38
Figure. 9	Optimal measurement delay calculated using least-square optimization.	39
Figure. 10	MSF estimated position with the GPS-based cutoff [(a) and (b)], and with the proposed GPS quality indicator algorithm [(c) and (d)].	40
Figure. 11	The MSF estimated position without the smoothing offset [(a) and (b)], and with the proposed smoothing offset algorithm [(c) and (d)].	41
Figure. 12	MSF estimated position covariance (a) and velocity covariance (b).	41
Figure. 13	The testing ground and flight trajectories (a) in the flight environment (b).	42
Figure. 14	Above-ground level (AGL) estimated from without outlier rejection (a) and with outlier rejection using Mahalanobis distance check (b).	42
Figure. 15	Vision pre-scale process that includes accelerometer and gyroscope biases.	43
Figure. 16	2D satellite google map overlay on 3D cloud points from the modified ORB_SLAM2 algorithm.	43

## List of Abbreviations and Symbols

AGL	Above-ground level.
AHRS	Attitude and heading reference system.
BRIEF	Binary robust independent elementary features.
DOF	Degree of freedoms.
EKF	Extended Kalman filter.
FAST	Features from accelerated segment test.
GPS	Global positioning system.
HACC	Horizontal accuracy estimate.
HDOP	Horizontal dilution of precision.
IEKF	Indirect Extended Kalman filter.
INAV	Inertial Navigation framework.
INS	Inertial Navigation System.
MEMS	Microelectromechanical systems.
MPC	Model predictive control.
MSF	Multi-sensor fusion.
NAV	Navigation.
ORB	Oriented FAST and rotated BRIEF.
PID	Proportional–integral–derivative
RL	Robot Localization framework.
ROS	Robot Operating System.
SLAM	Simultaneous localization and mapping.
SVD	Singular value decomposition.
UAV	Unmanned Aerial Vehicle.
UKF	Unscented Kalman Filter.
VACC	Vertical accuracy estimate.
VDOP	Vertical dilution of precision.
VIS	Position generated by vision measurement.
$\Delta t$	Difference between each time step.
$\Delta T$	Time difference between two consecutive keyframes.
$\mathbf{0}_{n \times n}$	The zero matrix.

$\mathbf{a}_m$	Acceleration measurement from accelerometer.
$\mathbf{a}_B$	Acceleration with respect to body frame.
$\mathbf{a}$	Acceleration with respect to world frame.
$\mathbf{b}_a$	Accelerometer bias.
$\mathbf{b}_\omega$	Gyroscope bias.
$corr_p$	Correction of the position state from GPS measurement.
$corr_v$	Correction of the velocity state from GPS measurement.
$\mathbf{C}_{wi}$	Rotational matrix of IMU frame with respect to world frame.
$\mathbf{C}_{vi}$	Rotational matrix of IMU with respect to vision frame.
$\mathbf{C}_{if}$	Rotational matrix of optical flow sensor offset to IMU frame.
$D$	Criteria function of GPS cut-off indicator.
$\mathbf{F}$	IMU system dynamic.
$\mathbf{g}$	Gravity vector.
$h$	Height measured from terrain to UAV.
$\mathbf{H}$	Linearized sensor measurement model.
$\mathbf{h}(\mathbf{x})$	Sensor measurement model.
$\mathbf{I}_{n \times n}$	The identity matrix.
$\mathbf{J}_{(\cdot)}^a$	Jacobian of changing accelerometer bias
$\mathbf{J}_{(\cdot)}^\omega$	Jacobian of changing gyroscope bias.
$\mathbf{K}$	Kalman gain.
$\hat{\lambda}$	Estimated vision measurement scale.
$\lambda$	Vision measurement scale.
$\mathbf{n}_{(\cdot)}$	White Gaussian noise of subscripted variable.
$\boldsymbol{\omega}_t$	3D rotational rate of UAV at time step t.
$\mathbf{p}_{gps}$	GPS position measurement.
$\mathbf{P}$	Error-state covariance matrix.
$\hat{\mathbf{P}}$	Estimated error-state covariance matrix.
$\hat{\mathbf{p}}_{wv}$	Estimated position of vision respected to world frame.
$\mathbf{p}_{ip}$	Estimated position offset of GPS sensor with respect to world frame.
$\hat{\mathbf{p}}_{wi}$	Estimated position state of IMU with respect to world frame.
$p_{wi,z}$	Height of UAV with respect to world frame.
$\mathbf{p}_{vc}$	Position of camera frame with respect to vision frame.



$\mathbf{p}_{ci}$	Position of IMU frame with respect to camera frame.
$\mathbf{p}_{vi}$	Position of IMU with respect to vision frame.
$\mathbf{p}_{wv}$	Position of vision respected to world frame.
$\mathbf{p}_{wi}$	Position state of IMU with respect to world frame.
$\Delta \mathbf{P}$	Smooth offset of UAV estimated position.
$\hat{\mathbf{p}}_t$	UAV estimated position state at time step $t$ .
$\mathbf{p}_t$	UAV position state at time step $t$ .
$\bar{\mathbf{p}}_{vc}$	Vector part quaternion orientation of vision frame with respect to IMU frame.
$\mathbf{Q}$	Covariance matrix.
$\hat{\mathbf{q}}_{wi}$	Estimated quaternion orientation of IMU with respect to world frame.
$\mathbf{q}_t$	Orientation of UAV represented in quaternion at time step $t$ .
$\mathbf{q}_{vc}$	Quaternion orientation measurement from SLAM system.
$\mathbf{q}_{ic}$	Quaternion orientation of camera frame with respect to IMU frame.
$\mathbf{q}_{wi}$	Quaternion orientation of IMU frame with respect to world frame.
$\mathbf{q}_{wv}$	Quaternion orientation offset of the vision frame with respect to world frame.
$\mathbf{R}_{WB}$	Rotational matrix of body frame respected to world frame.
$\mathbf{R}$	Covariance of measurement.
$\mathbf{S}$	Selection matrix.
$score_k$	Accumulated score from criteria function.
$\sigma_{bounded}$	Constrained HACC variance.
$\sigma$	Covariance.
$s$	Scale of camera trajectory.
$tz$	Estimated terrain height.
$\theta$	Orientation of UAV represented in quaternion except w-axis.
$\theta_{if}$	Orientation offset of optical flow sensor with respect to IMU frame.
$\delta \theta$	Vector part quaternion small change orientation of UAV.
$\theta_{wi}$	Vector part of orientation represented by quaternion state.
$\mathbf{V}_{gps}$	GPS velocity measurement.
$\hat{\mathbf{v}}_{wi}$	Estimated velocity of IMU frame with respect to world frame.
$\hat{\mathbf{v}}_t$	UAV estimated velocity state at time step $t$ .
$\mathbf{v}_t$	UAV velocity state at time step $t$ .
$\mathbf{v}_{vi}$	Velocity of IMU with respect to vision frame.

$\mathbf{v}_{wi}$	Velocity state of IMU with respect to world frame.
$W_p$	GPS position measurement weight.
$W_v$	GPS velocity measurement weight.
$\tilde{\mathbf{x}}_t$	UAV error-state at time step $t$ .
$\hat{\mathbf{x}}_t$	UAV estimated-state at time step $t$ .
$\mathbf{x}_t$	UAV true state at time step $t$ .
$\tilde{\mathbf{x}}_t^+$	Updated error-state at time step $t$ .
$\mathbf{y}$	Analytics residual.
$\tilde{\mathbf{z}}$	Error measurement model.
$\hat{\mathbf{z}}$	Estimated measurement model.
$\mathbf{z}_t$	Measurement model at time step $t$ .

## List of Publications

The list of publications was sorted in order of the study.

1. Publication of conference paper

Thanabadee Bulunseechart and Pruittikorn Smithmaitrie, Comparison of state estimation algorithms for autonomous GPS-Inertial navigation for UAV application, The 8th PSU-UNS International Conference on Engineering and Technology (ICET-2017), June 8-10, 2017, Novi Sad, Serbia.

(Open access reprinted)

2. Publication of journal article

Thanabadee Bulunseechart, and Pruittikorn Smithmaitrie 2018 A Method for UAV Multi- Sensor Fusion 3D- Localization under Degraded or Denied GPS Situation. *Journal of Unmanned Vehicle Systems*. 6(3): 155-176. doi:10.1139/juvs-2018-0007

(Reprinted with permission of NRC Research Press journal)

## Reprint were made with permission from publisher

**Publication of journal article:** A Method for UAV Multi-Sensor Fusion 3D-Localization under Degraded or Denied GPS Situation.

**Article**
« Previous TOC Next »

### A method for UAV multi-sensor fusion 3D-localization under degraded or denied GPS situation

Thanabadee Bulunseechart, Pruittikorn Smithmaitrie







Department of Mechanical Engineering, Faculty of Engineering, Prince of Songkla University, Hat Yai, Songkhla 90112, Thailand.

**Corresponding author:** Pruittikorn Smithmaitrie (e-mail: [pruittikorn.s@psu.ac.th](mailto:pruittikorn.s@psu.ac.th)).

Copyright remains with the author(s) or their institution(s). Permission for reuse (free in most cases) can be obtained from [RightsLink](#).

**Published on the web 12 July 2018.**

Received February 14, 2018. Accepted July 4, 2018.

-  [Abstract](#)
-  [PDF \(2974 K\)](#)
-  [PDF-Plus \(1723 K\)](#)
-  [Figures](#)
-  [Tables](#)
-  [References](#)

---

*Journal of Unmanned Vehicle Systems*, 2018, 6(3): 155-176, <https://doi.org/10.1139/juvs-2018-0007>

### Reprints and permissions for reuse of published material

Anyone may reuse figures, tables, and short excerpts from any NRC Research Press article, for any non-commercial use that respects the moral rights of authors, at no charge and without permission. However, if a license is required, one can be obtained for free by following the instructions below. In either case, the original publication should be acknowledged with a credit line that includes the author, article title, journal title, volume number, issue number, and the inclusive pages. The credit line must also include the wording "© Canadian Science Publishing or its licensors", except when an author of an original article published in 2009 or later is reproducing his/her own work.

**The process for permissions to reproduce Monographs content remains unchanged and instructions can be found from the Contact Us & Customer Support section.**

## **Introduction**

The unmanned aerial vehicle (UAV) is a flying machine that it being used for scientific, public and commercial purposes such as agriculture farming, surveillance, mapping, search and rescue mission, firefighting survey, medical transportation, aerial photogrammetry, inspection of power lines, weather forecast from atmospheric analysis, traffic monitoring in urban areas and etc.

There are two main types of UAV: heavier-than-air (e.g., fixed wing, rotary wing) and lighter-than-air (e.g., balloon) categorized by how lift is produced. The fixed wing UAV uses airspeed through the wing to produce the lift. The rotary wing UAV uses spinning rotor with airfoil section blades to produce the lift. The lighter-than-air use buoyancy to float in the air.

The UAVs take an advantage of manned aircraft by removing onboard pilot and pilot support systems to increase endurance, loiter time and allow deployment on high risk situations. The most important technology of UAV is the autonomous system. The faster decision-making ability than pilot, accurate sensing and situation awareness are trends of research and development according to increasing power of processing onboard controller.

The static hovering and capable of vertical take-off and landing of the rotary wing UAV, overcome the fixed wing UAV that use a large area to take-off and landing. The most popular rotary wing UAV is the multi-copter that contained more than three rotors to produce the lift and to

balance the thrust direction for stabilization. The multi-copter is also compactness and has less mechanic components to failure than the helicopter UAV. This makes a multi-copter suitable for many applications.

Because of UAV is a highly dynamic system, the various types of sensors and a robust controller must be carefully designed. That is a microprocessor with sensors integration, called the flight controller. The UAV controller has been studied and develop to control the orientation (or attitude), acceleration, velocity and position such as proportional-integral-derivative (PID) controller, sliding mode controller, linear-quadratic regulator (LQR) controller, back-stepping controller and etc. In general, the orientation, velocity and position are separately controlled. Often, the P-PID-controller is used for orientation control, P-controller for velocity control and P-controller for position control. In this thesis, the flight control is sufficiently elaborated by a Pixhawk<sup>1</sup> flight controller.

Although the UAV is in control, the UAV controller may not recognize the drifted position data from accumulated error of itself. Many non-drift sensors are used to compensate this situation such as global positioning system (GPS), laser scanner, camera, beacon, accelerometer for gravitation alignment and etc. Often, these sensors cannot be used alone for UAV navigation due to noise and some individual limitation, for examples GPS cannot be used in obstructed satellite areas, laser scanner cannot be used in unstructured area, camera cannot be used when low ambient light or non-feature area. Thus, the sensor fusion algorithms are

---

<sup>1</sup> Pixhawk, <https://pixhawk.org/>

developed by integrating those advantages to overcome each limitation and improve the UAV state estimation.

In the past, the GPS/IMU based state estimation was well designed to complete most of autonomous tasks but the drawback is that the GPS requires clean signal and usually fails when operate indoor or in obstructed satellite area. The ideal UAV should suite to assist the pilot control even in urban or cluttered environments. Many researches focus on correcting the GPS denied situation by using camera sensor and IMU fusion. There are some popular visual odometry software packages for ROS (Robot Operating System) such as SVO (Forster et al. 2014), DSO (Engel et al. 2016), and visual-inertial odometry such as ROVIO (Bloesch et al. 2015) which are robust and able to localize a UAV under indoor environment in real-time.

However, operation with visual odometry for a long duration under same location may increase positioning error. Simultaneous localization and mapping (SLAM) was used to solve this problem with capability in mapping and reutilizing the map data. Many effective SLAM methods are available as open source software, e.g., TUM\_ARDRONE (Engel, Sturm, et al. 2014), LSD\_SLAM (Engel, Schöps, et al. 2014) and Visual-Inertial ORB-SLAM (Mur-Artal & Tardós 2017). Nevertheless, their main drawback is that they have the greater re-projection error of each pixel in the larger scene when it operates outdoor (Hutchison et al. 2010; Weiss et al. 2011; and Chowdhary et al. 2013). This leads to inaccurate map estimation and unstable trajectories. The large re-projection error also induces the incorrect map scale estimation which unsuitable for positioning

control of the UAV. To overcome this problem, some additional sensors such as the GPS sensor must be added to enhance global trajectory consistency and scale correction.

The main objective of this thesis is to study and develop an IMU-based model state estimation algorithm for 3D UAV localization between indoor-outdoor transitions to improve ability of operate in GPS denied and degrade areas. This thesis divided into two parts. The first part is to find and compare appropriate state estimations that are currently available. The second part is to design an algorithm based on the selected state estimation to achieve the objective.

In first part, in order to estimate position of an UAV which is a nonlinear dynamic system, fast response and less computational burden are important requirements. The performance comparison of three state estimation algorithms: inertial navigation, robot localization and Ethzasl MSF frameworks is deployed and discussed in Chapter 2. The experimental results show that Ethzasl MSF framework has outperformed good estimation response, acceptable accuracy and reasonable computational burden. Moreover, its flexibility allows users to add other sensory information to extend the system capability to achieve the thesis goal.

In the second part, an algorithm of 3D-localization during transition between indoor and outdoor environments for a UAV is presented in Chapter 3. Localization inputs are based on information from GPS, IMU, pressure sensor, monocular camera and optical flow sensor. The



information is carefully selected using GPS quality indicator method regarding to the operating environment. After that, the smoothing offset approach is employed to smooth the position estimation. The selected sensor data are filtered by indirect extended Kalman filter for localization and extrinsic sensor calibration in real-time. Results show a seamless offset convergence of UAV localization for indoor-outdoor transition. Moreover, the proposed method of decision-making to cutoff GPS measurement even when it experiences poor signal quality can still outperform conventional GPS-based cutoff method in terms of response time.

In conclusion, the UAV state estimation along with GPS quality indicator for indoor-outdoor transition and pre-scale vision handling have been studied. The proposed algorithm is successfully implemented to navigate the UAV with low-cost sensors platform between high rise building and outdoor. In field test, the result shown seamless transition between building and outdoor area, give reasonable trajectory and perform GPS recovery when available. In the future, this MSF work might be further improved by adding on more sensor measurements to assist UAV state estimation in more complex tasks, such as avoidance of moving objects.

**Publication of conference paper:**

Thanabadee Bulunseechart and Pruittikorn Smithmaitrie,  
Comparison of state estimation algorithms for autonomous GPS-Inertial  
navigation for UAV application, *The 8th PSU-UNS International  
Conference on Engineering and Technology (ICET-2017)*, June 8-10,  
2017, Novi Sad, Serbia.  
(Open access reprinted)



The 8<sup>th</sup> PSU-UNS International Conference on Engineering and Technology (ICET-2017), Novi Sad, Serbia, June 8-10, 2017  
University of Novi Sad, Faculty of Technical Sciences

# COMPARISON OF STATE ESTIMATION ALGORITHMS FOR AUTONOMOUS GPS-INERTIAL NAVIGATION FOR UAV APPLICATION

Thanabadee Bulunseechart and Pruittikorn Smithmaitrie\*

Department of Mechanical Engineering, Faculty of Engineering,  
Prince of Songkla University, Hat Yai, Songkla 90112, Thailand

\*E-mail: spruitti@me.psu.ac.th

**Abstract:** In order to estimate position of an unmanned aerial vehicle (UAV) which is a nonlinear dynamic system, accuracy, fast response and less computational burden are important requirements. This work compares performance of three state estimation algorithms: inertial navigation, robot localization and Ethzasl MSF frameworks. They are implemented on ROS (Robot Operating System) to control the same UAV platform. In the experiment, GPS measurement is referred as absolute ground position for short and long flight dataset. Then, the state estimators are investigated in term of accuracy, speed and computational burden. The experimental results show that Ethzasl MSF framework has outperformed good estimation response, acceptable accuracy and reasonable computational burden. Moreover, its flexibility allows users to add other sensory information for complex scenarios.

**Key Words:** State estimation; UAV navigation; EKF; GPS; Inertial Nav; Robot localization; Multi-sensor fusion.

## 1. INTRODUCTION

An unmanned aerial vehicle (UAV) or “drone” is widely used for aerial-photography, 3D-mapping, transportation and etc. Most applications require a good navigation system to assist pilot operation. Many research works can be found in this field and many open-source software packages are available.

The most common state estimation method is to combine INS (Inertial Navigation System) with GPS (Global Positioning System) information for merging benefits of INS and GPS and reducing their errors as shown in Table 1 [1]. INS is suitable for highly dynamic navigation but trends to drift over time, whereas GPS can bound the error but it has slow and fluctuated response.

Using both together can improve performance of the navigation system than either one alone [2].

**Table 1.** Advantages and drawbacks of INS and GPS

	INS	GPS
<b>Measurement frequency</b>	High	Low
<b>Error accumulate</b>	Unbounded	Bounded
<b>Dynamic response</b>	Good	Bad
<b>Jamming susceptibility</b>	Very low	High
<b>Attitude information</b>	Available	Not available

Challenges for this state estimation apart from its accuracy are speed of the state estimation, multi-frequency and multi-delay measurement handling e.g. various samplings of visual and GPS information. Furthermore, flexibility of adding other sensory information is advantage to be improved for navigation performance. The main goal of this research is to compare the three open-source state estimations that are based on INS and GPS. They are the Inertial Nav (INAV)<sup>1</sup>, robot\_localization (RL)<sup>2</sup> and Ethzasl MSF frameworks. (MSF)<sup>3</sup>. In summary, a proposed sensing technique that developed based on MSF can significantly improve the state estimation result. Detail of the algorithms, performance criteria, experimental setup based results and conclusion are respectively presented next.

## 2. STATE ESTIMATION ALGORITHMS

Inertial navigation, robot localization and MSF estimations require two measurement models. First, the measurement model of GPS ( $z_t$ ) that consists of 2-D position ( $p_{gps}$ ) and velocity ( $v_{gps}$ ) measurements. It can be written as

<sup>1</sup> PX4 autopilot firmware, <https://github.com/PX4/Firmware/>

<sup>2</sup> robot\_localization, [http://wiki.ros.org/robot\\_localization](http://wiki.ros.org/robot_localization)

<sup>3</sup> Ethz-asl MSF framework, [http://wiki.ros.org/ethzasl\\_sensor\\_fusion](http://wiki.ros.org/ethzasl_sensor_fusion)

$$z_{gps,t} = \begin{bmatrix} p_{gps} \\ v_{gps} \end{bmatrix} + n_{gps} \quad (1)$$

where  $n_{gps} = \begin{bmatrix} n_{gps,p} \\ n_{gps,v} \end{bmatrix}$  is white Gaussian noise of GPS measurement. Second, an inertial measurement based on accelerometer can be expressed as

$$a_m = a_B + n_a + b_a \quad (2)$$

where  $a_m$  is the measured acceleration of accelerometer sensor,  $a_B$  is the acceleration that expressed in body frame,  $n_a$  is white Gaussian noise and  $b_a$  is the accelerometer bias. Later, these two measurement models will be inputs to estimate the position state for all studied algorithms.

### 2.1 The inertial navigation (INAV)

INAV is one of accurate state estimators that used in PX4 firmware [3]. It has an advantage of a compact code that is compatible with cheap microcontrollers such as Arduino. It utilizes both GPS position and velocity measurements to estimate the 3DOF position of an UAV by compensating the measurement delay as shown in Fig. 1.

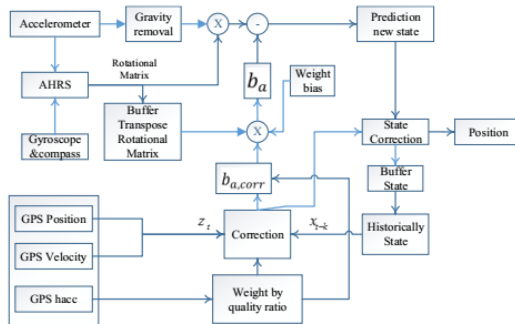


Fig. 1. The INAV algorithm used in PX4 firmware.

The body acceleration  $a_B$  can be determined by Eq. (2). Then, the body acceleration relative to the earth frame ( $a$ ) can be obtained by

$$a = R_{EB} a_B \quad (3)$$

where  $R_{EB}$  is the rotational matrix which can be obtained from the attitude and heading reference system (AHRS) [4]. The state variable ( $x_t$ ) consists of position ( $p_t$ ) and velocity ( $v_t$ ) vectors in current time step  $t$  that relative to the earth frame as

$$x_t = [p_t^T \quad v_t^T]^T \quad (4)$$

In general, the position and velocity vectors have three components in the x, y and z directions. However, in practice, the estimations are calculate only in x and y components because the measured GPS in the z direction has too much fluctuation at low altitude [5]. First, before any correction, the initial state is estimated by

$$\hat{p}_t = p_{t-1} + v_{t-1} \Delta t + \frac{1}{2} S R_{EB} a_B \Delta t^2 \quad (5)$$

$$\hat{v}_t = v_{t-1} + S R_{EB} a_B \Delta t \quad (6)$$

where  $\hat{p}_t$  is the predicted position,  $\hat{v}_t$  is the predicted velocity and  $S = [I_{2 \times 2} \quad \mathbf{0}_{2 \times 1}]$  is a  $2 \times 3$  selection matrix. The hat sign means that the state has not been adjusted by the correction step.

After the GPS information is available, the correction ( $corr$ ) of the state can be determined by the difference between the state at the current iteration ( $t$ ) and the state at the ( $t - k$ ) iteration as written in Eqs (7) and (8) where and  $k$  is the number of iteration that corresponds to the delayed time of the measurement.

$$corr_p = p_{gps,t} - p_{t-k} \quad (7)$$

$$corr_v = v_{gps,t} - v_{t-k} \quad (8)$$

Similarly, the accelerometer bias ( $b_{a,t}$ ) can also be corrected as

$$b_{a,t} = b_{a,t-1} + R_{EB,t-k} b_{a,corr} \quad (9)$$

where

$$b_{a,corr} = -(corr_p W_p^2 + corr_v W_v) \quad (10)$$

Consequently, the position and velocity states are respectively predicted as

$$p_t = \hat{p}_t + corr_p W_p \Delta t + corr_p W_p^2 \Delta t^2 \quad (11)$$

$$v_t = \hat{v}_t + corr_v W_v \Delta t \quad (12)$$

where  $W_p$  and  $W_v$  are the position and velocity GPS weight functions, respectively. They are determined by GPS standard deviation  $\sigma_{xy}$  for state correction as

$$W_p = c_p \frac{\sigma_{xy,min}}{\max(\sigma_{xy}, \sigma_{xy,min})} \quad (13)$$

$$W_v = c_v W_p \quad (14)$$

where  $c_p$  and  $c_v$  are the positive constants and  $\sigma_{xy,min}$  is the minimum acceptable GPS standard deviation. Then, state variables  $p_t$  and  $v_t$  will be stored for the next prediction and correction.

### 2.2 The robot localization (RL)

The RL is a software package for nonlinear state estimation developed by Charles River Analytics. It operates under Robot Operation System (ROS) [6]. The package contains an implementation of 6DOF nonlinear state estimators that consists of Extended Kalman Filter (EKF) and Unscented Kalman Filter (UKF). In this work, the UKF for 6DOF estimation is implemented. The 15-state variable  $x_t$  composed of state vectors relative to the earth frame is

$$x_t = [p_t^T \quad q_t^T \quad v_t^T \quad \omega_t^T \quad a_t^T]^T \quad (15)$$

where  $p_t$  is the position state vector,  $q_t$  is the Euler attitude state vector,  $v_t$  the velocity state vector,  $\omega_t$  is the

angular velocity state vector and  $a_t$  is the linear acceleration state vector.

The RL utilizes information from sensors according to ROS format. It supports relative measurement such as IMU, odometry sensors (e.g. wheel-travelled distance and vision velocity) that subjected to increase error in time, and absolute measurement (e.g. GPS, VICON) as shown in Fig. 2. This study uses the position  $p_t$  and velocity  $v_t$  measurements from GPS, while the attitude  $q_t$  and acceleration  $a$  are from AHRS algorithm and IMU respectively.

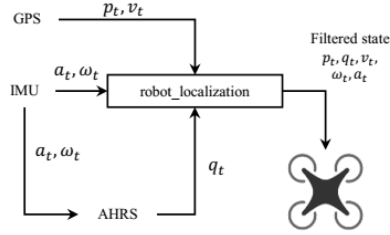


Fig. 2. Sensor measurement and state variables of the robot localization package<sup>4</sup>

### 2.3 The modified MSF framework (MSF)

Ethzasl MSF framework is also a ROS software package that was developed by Eidgenössische Technische Hochschule Zürich. It contains time delay compensation for single and multi-sensor fusion based on an indirect (error-state) EKF for nonlinear 6DOF pose estimation including intrinsic and extrinsic sensor calibrations. The EKF is divided into the two stages: prediction and update. The prediction is modelled based on IMU measurement. This means that the framework can be implemented on any robot that has IMU. The detail algorithm of this framework can be found in [7].

In this work, the nominal state  $x_t$  is defined with the 16-element variables relative to the earth frame as

$$x_t = [p_t^T \quad v_t^T \quad q_t^T \quad b_{\omega,t}^T \quad b_{a,t}^T]^T \quad (16)$$

where  $p_t$  is the IMU position,  $v_t$  is the IMU velocity,  $q_t$  is the IMU attitude,  $b_{\omega,t}$  is the gyro biases and  $b_{a,t}$  is the accelerometer biases. The 15 elements of the error-state can be written as

$$\tilde{x}_t = [\Delta p_t^T \quad \Delta v_t^T \quad \delta \theta_t^T \quad \Delta b_{\omega,t}^T \quad \Delta b_{a,t}^T]^T \quad (17)$$

where the error-state for non-quaternion components can be determined by the difference between the true state  $n$  and estimated state  $\hat{n}$  as

$$\Delta n = n - \hat{n} \quad (18)$$

where  $n \in \{p_t, v_t, b_{a,t}, b_{\omega,t}\}$ . In Hamilton representation of the quaternion [8], the quaternion error  $\delta q$  can be described in term of the rotational vector  $\delta \theta$  [9] as

$$\delta q = q \otimes \hat{q} \approx \begin{bmatrix} 1 \\ \frac{1}{2} \delta \theta \end{bmatrix} \quad (19)$$

The nominal state are predicted by using the 2<sup>nd</sup> order Taylor truncation integration as follows,

$$p_t = p_{t-1} + v_{t-1} \Delta t + \frac{1}{2} (R_{EB}(a_{m,t-1} - b_{a,t-1}) + g) \Delta t^2 \quad (20)$$

$$v_t = v_{t-1} + (R_{EB}(a_{m,t-1} - b_{a,t-1}) + g) \Delta t + v_n \quad (21)$$

$$q_t = q \otimes q\{(\omega_{m,t-1} - b_{\omega,t-1}) \Delta t + \theta_n\} \quad (22)$$

$$b_{\omega,t} = b_{\omega,t-1} + b_{\omega n} \quad (23)$$

$$b_{a,t} = b_{a,t-1} + b_{a n} \quad (24)$$

where  $R_{EB} \triangleq R_{EB}\{q_t\}$  is the rotational matrix that can be obtained from quaternion  $q_t$ ,  $\omega_{m,t-1}$  is the angular velocity that measured from gyroscope unit at time step  $t$ ,  $v_n, \theta_n, b_{\omega n}$  and  $b_{a n}$  are the Gaussian noises of velocity, orientation and estimated biases, respectively. The indirect EKF prediction step of the error-state can be summarized as

$$\hat{\tilde{x}}_t = F_{D,t} \tilde{x}_{t-1} \quad (25)$$

$$\hat{P}_t = F_{D,t} P_t F_{D,t}^T + Q_{D,t} \quad (26)$$

where  $F_{D,t}$  and  $Q_{D,t}$  are the discretized Jacobian matrixes of IMU model,  $P_t$  is the previous error-state covariance matrix,  $\hat{P}_t$  is the predicted error-state covariance matrix and  $Q_D$  is the covariance matrix in discrete time, which has been presented in [10].

When the measurement is available, each update follows the same procedure as expressed in Eq. (27) through Eq. (30).

$$y_t = z_t - \hat{z}_t \quad (27)$$

$$K_t = \hat{P}_t H_t^T (H_t \hat{P}_t H_t^T + R_t)^{-1} \quad (28)$$

$$\tilde{x}_t^+ = K_t y_t \quad (29)$$

$$P_{t+1} = (I - K_t H_t) \hat{P}_t \quad (30)$$

where  $y_t$  is the analytic residual,  $z_t$  is the measurement,  $\hat{z}_t$  is the measurement from the model,  $H_t$  is the Jacobian of the analytic residual with respect to the error-state,  $K_t$  is the Kalman gain,  $P_{t+1}$  is the propagated error-state covariance and  $R_t$  is the covariance of measurement. The updated error-state  $\tilde{x}_t^+$  is injected to the nominal state  $x$  as

$$x_t = x \oplus \tilde{x}^+ \quad (31)$$

where the operator  $\oplus$  is defined by the following rules. First, all states except quaternion states can be determined by  $x_t = x_{t-1} + \Delta x^+$  and second, quaternion can be determined by  $q_t = q_{t-1} \otimes q\{\delta \theta_t^+\}$  [9].

Finally, the true state  $x_t$  and the updated error-state covariance matrix  $P_{t+1}$  is stored for the next iteration while the error-state is reset to zero.

#### 2.3.1 GPS error measurement model

A 2-D GPS velocity measurement handler Eq.(1) is added into the framework in order to fuse with GPS

<sup>4</sup> robot localization package, [http://wiki.ros.org/robot\\_localization](http://wiki.ros.org/robot_localization)

measurement. Then, the GPS error measurement model can be written as

$$\tilde{z}_{gps,t} = \begin{bmatrix} \Delta p_{gps} \\ \Delta v_{gps} \end{bmatrix} + \begin{bmatrix} n_{gps,p} \\ n_{gps,v} \end{bmatrix} \quad (32)$$

where  $n_{gps,p}$  is the white Gaussian noise of GPS position and  $n_{gps,v}$  is the white Gaussian noise of GPS velocity. The GPS measurement error model can be linearized as

$$\tilde{z}_{gps,t} = H_{gps} \tilde{x}_t + R_{gps,t} \quad (33)$$

where  $H_{gps}$  denotes the Jacobian of the GPS measurement with respect to the error-state.

$$H_{gps} = \begin{bmatrix} I_{2 \times 2} & \mathbf{0}_{2 \times 1} & \mathbf{0}_{2 \times 2} & \mathbf{0}_{2 \times 10} \\ \mathbf{0}_{2 \times 2} & \mathbf{0}_{2 \times 1} & I_{2 \times 2} & \mathbf{0}_{2 \times 10} \end{bmatrix} \quad (34)$$

The measurement covariance  $R_{gps,t}$  can be written as

$$R_{gps,t} = \text{diag}[\sigma_{p,t}^2, \sigma_{v,t}^2] \quad (35)$$

where  $\sigma_{p,t}$  is the horizontal position standard deviation and  $\sigma_{v,t}$  is the horizontal speed standard deviation. They can be obtained directly from GPS information.

Mahalanobis test is implemented to reject the GPS measurement outlier before applying the update to the error-state. In general, the Mahalanobis distance  $d$  may not always be positive, it has to be modified by forcing the error-state covariance matrix  $P$  to be the symmetric matrix as follow,

$$d_t = y_t^T (H_{gps} P_t H_{gps}^T + R_{gps,t})^{-1} y_t \quad (36)$$

where  $d_t$   $P_{s,t}$  is the symmetric covariance matrix that can be obtained by  $P_{s,t} = \frac{1}{2}(P_t + P_t^T)$ .

### 2.3.2 Attitude error measurement model

GPS measurement does not provide reliable attitude observation. Thus, the Mahony's AHRS algorithm [4] is adopted as an estimated observed attitude measurement. The attitude error  $\tilde{z}_{ahrs}$  can be defined as [9]

$$\tilde{z}_{ahrs} = \frac{1}{2} \begin{pmatrix} \tilde{q}_{vec} \\ \tilde{q}_w \end{pmatrix} \quad (37)$$

where  $\tilde{q}_{vec}$  is the pure quaternion and  $\tilde{q}_w$  is the real quaternion. The analytic residual  $\tilde{q}$  can be computed by using multiplication [11] instead of using subtraction [12] as

$$\tilde{q} = q^* \otimes q_{ahrs} \quad (38)$$

where  $q_{ahrs}$  is the AHRS attitude measurement. The attitude error can be linearized as

$$\tilde{z}_{ahrs,t} = H_{ahrs} \tilde{x}_t + R_{ahrs,t} \quad (39)$$

where

$$H_{ahrs} = [\mathbf{0}_{3 \times 6} \quad I_{3 \times 3} \quad \mathbf{0}_{3 \times 6}] \quad (40)$$

$$R_{ahrs,t} = \sigma_{q,t}^2 [I_{3 \times 1}] \quad (41)$$

where  $\sigma_{q,t}$  is the orientation standard deviation which can be obtained from Mahony's AHRS algorithm in [13].

### 3. EXPERIMENTAL SETUP

All proposed algorithms are tested on a quadrotor UAV as shown in Fig. 3. The flight control board is developed based on PX4 firmware autopilot [3]. The Pixhawk<sup>5</sup> board consists of an IMU (3-axis accelerometer+gyroscope (MEMS-IMU, MPU6000), internal/external compass (HMC5883L), barometric sensor (MS5611) and external GPS (Ublox NEO-7N). The state estimation and trajectory generation are processed by an Odroid U3 computer with 1.7GHz Quad-Core processor and memory of 2 GB. The computer is installed on the UAV.

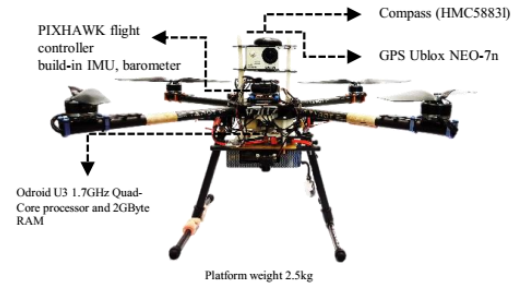


Fig. 3. The tested quadrotor UAV.

The desired velocity and trajectory are generated by a waypoint equation and sent to the Pixhawk flight controller. There are two flight testing paths: short and long travelling distance. The short flight path is an eight-shape trajectory and the UAV desired heading velocity is set at 0.6 m/s. The long flight path is a rectangular-shape trajectory (70m×100m) and the UAV travels with desired velocity of 2 m/s and stops at each corner. The short and long flight datasets (IMU, GPS, barometer and compass information) are recorded in ROS bag format<sup>6</sup>. Then, the flight datasets are fed to the state estimators as inputs. The estimation performance is investigated by means of position, accuracy and computation burden.

In order to validate the estimation accuracy, the GPS delayed time is shifted by 0.25 sec to compute the absolute ground position. The shift between the ground truth and the estimated position indicates the prediction accuracy. A computer with Intel Core i7-2630QM 2.00 GHz processor and memory of 2 GB is the shared platform for testing the computational burden of each state estimator. Flexibility of framework development is defined by ability of adding new sensory information with minimum coding.

<sup>5</sup> Pixhawk, <https://pixhawk.org/>

<sup>6</sup> rosbag, <http://wiki.ros.org/rosbag>

4. RESULTS

All state estimation frameworks are tested with the short flight trajectory compared with the ground truth. The result (Fig. 4) shows that the MSF framework has the best position estimation for the flight path with many turns in short distance.

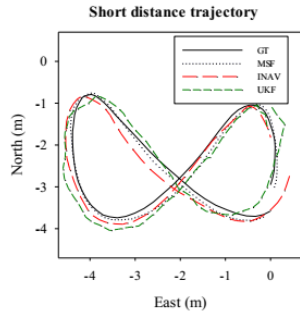


Fig. 4. Position estimation results of short flight testing.

The perimeter of the long flight path ground truth is about the size of a soccer field as shown in Fig. 5(left). In large scale view, state estimation results of each framework are very hard to distinguish (Fig. 5 (right)). Thus, the change of estimated position in time is plotted in small scale to compare the accuracy of the frameworks.

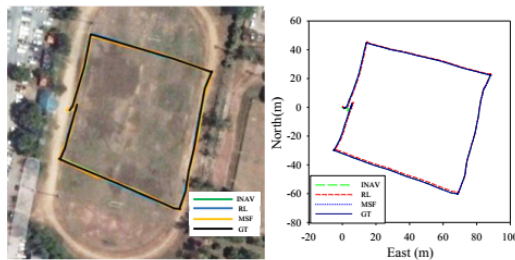


Fig. 5. Position estimation results of long flight testing in large scale view.

Position estimation and error compared with ground truth of the short and long flight tests are shown in Fig. 6 and 7, respectively. The modified MSF framework fusing with GPS velocity input provides the most accurate estimation for the short flight test (Fig. 6). However, the INAV provides the most accurate state estimation for the long flight test (Fig. 7). To quantify accuracy of state estimation algorithms, root-mean-square error (RMSE) of the position state is determined by comparing with the ground truth as reported in Table 2.

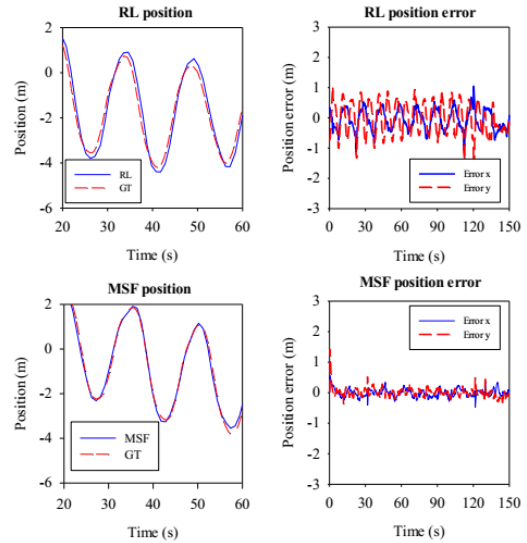
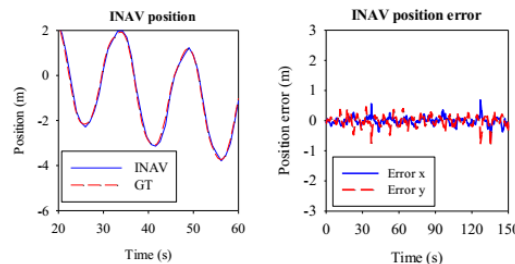


Fig. 6. Position estimation (x-direction) and error compared with ground truth of the short flight test.

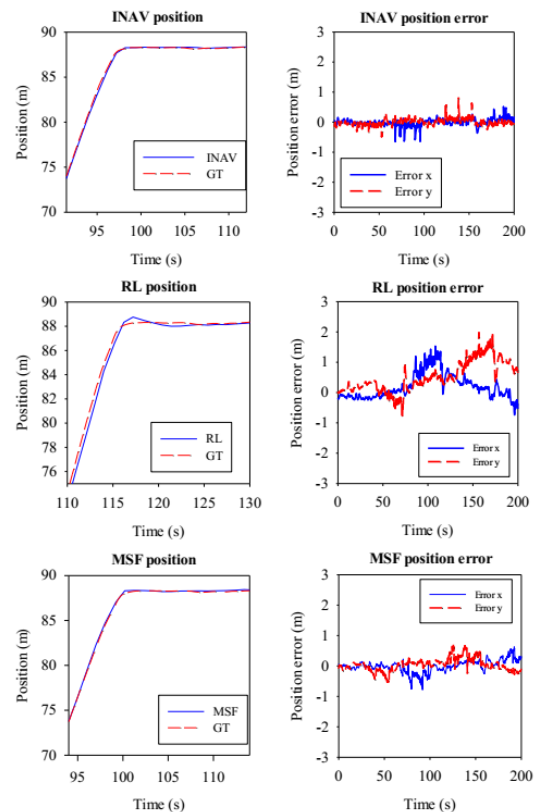


Fig. 7. Position estimation (x-direction) and error compared with ground truth of the long flight test.

Table 2. Root-mean-square error of position estimation

Algorithm	Short flight	Long flight
INAV	0.13	<u>0.12</u>
MSF	0.17	0.22

MSF+GPS velocity	<u>0.11</u>	0.18
RL	<u>0.44</u>	<u>0.45</u>

For speed estimation, both INAV and Modified MSF frameworks can predict the state before arrival of the GPS information, that is faster than that of the RL framework. It is because the INAV and MSF frameworks have the time-delayed compensation and the accelerometer/gyroscope bias correction as mentioned before.

The flexibility of framework is compared in Table 3. It shows that the MSF is the most flexible framework for adding other state variables or measurement types, such as INS, GPS or vision odometry. The MSF also supports the relative measurement handling on exteroceptive sensors such as laser scan or vision sensors [14].

Table 3. *Properties of frameworks*

	Delay compensated	Modification measurement matrix	Covariance handling	Mahalanobis distance	State extendable
INAV	Yes	No	Constant	No	No
MSF	Yes	Yes	Statistically	Yes	Yes
RL	No	No	Statistically	Yes	No

On the other hand, the RL framework utilizes UKF to avoid Jacobian matrix derivation for both prediction and correction steps. This causes the RL framework to have the highest computational burden as shown in Table 4. Hence, the RL framework is not suitable for the limited computational resource platform.

Table 4 *Computational burden.*

Algorithms	Rate	CPU Load
INAV	Up to IMU (100hz)	25%
MSF	Up to IMU (100hz)	38%
RL	15hz	112%

## 5. CONCLUSION

The three state estimation algorithms are evaluated and experimentally compared in this work. The MSF algorithm fusing with the GPS velocity information has the good position estimation, in term of accuracy, and flexibility of adding sensor inputs with the minimum work to convert measurement data to the state variables. Although the MSF has slightly lower accuracy in position estimation than that of INAV. This work is a guidance on choosing a suitable open-source framework for UAV navigation. Next, the MSF framework will be tested in complex situations such as outdoor-to-indoor flight.

## 6. REFERENCES

- [1] D.H. Titterton, J.L., "Strapdown Inertial Navigation Technology," in *American Institute of Aeronautics and Astronautics*, 2004.
- [2] D. J. Biezad, "Integrated Navigation and Guidance Systems," in *American Institute of Aeronautics and Astronautics*, 1999.
- [3] L. Meier, D. Honegger and M. Pollefeys, "PX4: A node-based multithreaded open source robotics

- framework for deeply embedded platforms," in *2015 IEEE International Conference on Robotics and Automation (ICRA)*, 2015.
- [4] Mahony, R., Hamel, T., and Pflimlin, J.M., "Nonlinear complementary filters on the special orthogonal.," in *IEEE Trans. on Automatic Control*, 2008.
- [5] Shi J, Cannon ME, "Critical error effects and analysis in carrier phase-based airborne GPS positioning over large areas.," *Bull Geod*, no. 69, pp. 261-273, 1995.
- [6] T. Moore, D. Stouch, "A Generalized Extended Kalman Filter Implementation for the Robot Operating System," in *Intelligent Autonomous Systems*, 2014.
- [7] Simon Lynen, Markus Achtelik, Stephan Weiss, Margarita Chli and Roland Siegwart, "A Robust and Modular Multi-Sensor Fusion Approach Applied to MAV Navigation.," in *IEEE/RSJ Intl. Conf*, 2013.
- [8] J. Kuipers, "Quaternions and Rotation Sequences," Princeton University Press, New Jersey, 1999.
- [9] J. Sola, "Quaternion kinematics for the error-state KF," Laboratoire d'Analyse et d'Architecture des Systemes- Centre national de la recherche scientifique (LAAS-CNRS), Toulouse, France, Tech., 2012.
- [10] S. Weiss, M. W. Achtelik, S. Lynen, M. C. Achtelik, L. Kneip, M. Chli and R. Siegwart, "Monocular vision for long-term micro aerial vehicle state estimation: A compendium," *Journal of Field Robotics*, vol. 30, pp. 803-831, 2013.
- [11] S. Weiss and R. Siegwart, "Real-Time Metric State Estimation for Modular Vision-Inertial Systems," in *IEEE Intl. Conf. on Robotics and Automation*, Shanghai, May 2011, pp. 4531–4537.
- [12] N. Trawny and S. I. Roumeliotis, "Indirect Kalman Filter for 3D Attitude Estimation A Tutorial for Quaternion Algebra," Multiple Autonomous Robotic Systems Lab, Tech. Rep. 612, 2005.
- [13] Cavallo A, Cirillo P, De Maria G, Falco P, Natale P, et al, "Experimental comparison of sensor fusion algorithms for attitude estimation.," in *Proceedings of the 19th IFAC World Congress 2014 (IFAC 2014)*, Cape Town (SA), 2014.
- [14] S. I. Roumeliotis and J. W. Burdick, "Stochastic cloning: A generalized framework for processing relative state measurements," in *Proc. of the*, Washington, DC, 2002.



**Publication of journal article:**

Thanabadee Bulunseechart, and Pruittikorn Smithmaitrie 2018 A Method for UAV Multi-Sensor Fusion 3D-Localization under Degraded or Denied GPS Situation. *Journal of Unmanned Vehicle Systems*. 6(3): 155-176. doi:10.1139/juvs-2018-0007

(Reprinted with permission of NRC Research Press journal)

# A method for UAV multi-sensor fusion 3D-localization under degraded or denied GPS situation

Thanabadee Bulunseechart and Pruittikorn Smithmaitrie

**Abstract:** Unmanned aerial vehicles (UAVs) have been developed to be used in complex environments. Continuity of a UAV operation when GPS is degraded or denied is crucial in many applications, such as flying near high buildings and trees, or flying outdoor-to-indoor. In this paper, an algorithm for 3D-localization during transition between indoor and outdoor environments for a UAV is presented. Localization inputs are based on information from GPS, inertial measurement unit, monocular camera, and optical flow sensor. Information is carefully selected using GPS quality indicator method corresponding to the operating environment. After that, a smoothing offset approach is employed to smooth the position estimation. The selected sensors' data are filtered by indirect extended Kalman filter for localization and extrinsic sensor calibration in real time. Results show a seamless offset convergence of UAV localization for indoor-outdoor transition. Moreover, the proposed method of decision-making to cut off GPS measurement even when it experiences poor signal quality can still outperform conventional GPS-based cutoff method in terms of response time.

**Key words:** sensor fusion, simultaneous localization and mapping (SLAM), unmanned aerial vehicles (UAV), global positioning system (GPS), GPS denied environments, Kalman filters, measurement of uncertainty.

**Résumé :** Les véhicules aériens sans pilote (UAV) ont été développés afin d'être utilisés dans des environnements complexes. La continuité du fonctionnement d'un UAV, dans le cas où le système de positionnement GPS est dégradé ou sans service, est cruciale dans un grand nombre d'applications comme le cas du vol d'un UAV près d'édifices en hauteur et d'arbres, ou de vol de l'extérieur à l'intérieur. Dans le cadre de cette étude, on présente un algorithme aux fins de la localisation tridimensionnelle pendant la transition d'un UAV entre des environnements intérieur et extérieur. Les saisies de localisation sont fondées sur des données de GPS, d'un appareil d'unité de mesure inertielle, d'un appareil-photo monoculaire et d'un capteur de flux optique. Les informations sont soigneusement choisies utilisant la méthode d'indicateur de la qualité GPS correspondant au contexte de manœuvre. Après cela, une approche de lissage des écarts est employée pour lisser l'évaluation de la position. Les données des capteurs choisis sont filtrées par le filtre de Kalman élargi indirect pour la localisation et l'étalonnage extrinsèque de capteurs en temps réel. Les résultats montrent une convergence uniforme des écarts de localisation d'UAV au niveau de la transition intérieure-extérieure. De plus, la méthode proposée de prise de décision quant au seuil de mesure de GPS, même quand celui-ci éprouve une faible qualité de signal, peut toutefois

Received 14 February 2018. Accepted 4 July 2018.

**T. Bulunseechart and P. Smithmaitrie.** Department of Mechanical Engineering, Faculty of Engineering, Prince of Songkla University, Hat Yai, Songkhla 90112, Thailand.

**Corresponding author:** Pruittikorn Smithmaitrie (e-mail: [pruittikorn.s@psu.ac.th](mailto:pruittikorn.s@psu.ac.th)).

Copyright remains with the author(s) or their institution(s). Permission for reuse (free in most cases) can be obtained from [RightsLink](https://www.rightslink.com).

surpasser la méthode traditionnelle d'établissement de seuil GPS, et ce, au niveau du temps de réponse. [Traduit par la Rédaction]

*Mots-clés* : fusion de données de capteurs, cartographie et localisation simultanées (« SLAM »), véhicules aériens sans pilote (UAV), système de localisation GPS, environnements sans service GPS, filtres de Kalman, incertitude de mesure.

## 1. Introduction

During the past several years, unmanned aerial vehicle (UAV) navigation research has been highly active for both indoor and outdoor applications. The main research goal is to improve UAV performance in many applications, such as agriculture farming, surveillance, mapping, search and rescue, and aerial photogrammetry. These applications require a robust state estimation of the UAV to cope with highly dynamic responses.

Many research works achieve good UAV state estimation for navigation with low-cost sensors (Lynen et al. 2013; Abeywardena et al. 2014; Burri et al. 2015; Leishman and McLain 2015; Santamaria-Navarro et al. 2015). Two major groups of dynamic models for state estimation algorithm are: the inertial measurement unit (IMU)-based approach (Lynen et al. 2013; Santamaria-Navarro et al. 2015) and the model-based approach (Abeywardena et al. 2014; Burri et al. 2015; Leishman and McLain 2015). The advantage of the IMU-based model is that UAV motion is directly modeled based on IMU information to avoid calculation complexity and to increase the ease of implementation on various types of sensor information. On the other hand, the model-based approach is a mathematical model of specific UAV dynamics. It is complicated to derive though it is more robust in terms of disturbance rejection and state estimator convergence.

Research on vision-based navigation systems has been increasingly conducted during the past several years. There are some popular visual odometry software packages for ROS (Robot Operating System) such as SVO (Forster et al. 2014), DSO (Engel et al. 2016), and visual-inertial odometry, such as ROVIO (Bloesch et al. 2015), which are robust and able to localize a UAV under indoor environment in real-time. However, operation with visual odometry for a long duration under the same location may increase positioning error. Simultaneous localization and mapping (SLAM) was used to solve this problem with its capability in mapping and reutilizing the map data. Many effective SLAM methods are available as open source software (e.g., TUM\_ARDRONE (Engel et al. 2014b), LSD\_SLAM (Engel et al. 2014a), and visual-inertial ORB-SLAM (Mur-Artal and Tardós 2017). Nevertheless, their main drawback is the greater re-projection error of each pixel of the larger scene (Hutchison et al. 2010; Weiss et al. 2011; Chowdhary et al. 2013) when it operates outdoors. This leads to inaccurate map estimation and unstable trajectories. The larger re-projection error also induces incorrect map scale estimation unsuitable for positioning control of the UAV. To overcome this problem, some additional sensors, such as a GPS sensor, must be added to enhance global trajectory consistency and scale correction.

The main goal of this work is to develop an algorithm for 3D UAV localization between indoor-outdoor transition environment similar to works presented by Nyholm (2015) and Shen et al. (2014). However, proprioceptive and exteroceptive methods are adopted to apply to low-cost sensors. The sensors are: a MEMS IMU (MPU6000), a barometric sensor (MEAS MS5611), and a magnetometer (ST Micro LSM303D), which are built in within a Pixhawk flight controller unit (Meier et al. 2012), GPS sensor (UBLOX NEO-7N), optical flow sensor (PX4FLOW), and CMOS camera (QUMOX-SJ4000). In this work, the UAV dynamics are modeled by the IMU model-based state estimation to lessen computational burden.

State estimation, based on indirect extended Kalman filter (IEKF) (Lynen et al. 2013), has an advantage of delay measurement compensation with good results in GPS outdoor

positioning, and that open-source code is also available. For indoor localization, the ORB-SLAM-inertial algorithm is implemented in the case of degraded or denied GPS measurements because its processed large-scale map can be reused to prevent drifting at recognized locations.

The anticipated benefit of this work is to expand the frontier of semi-autonomous UAV operation to more applications that involve unpredictable GPS quality environment. One example is the search and rescue application that uses a semi-autonomous UAV to survey a variety of areas: indoors, high-rise buildings, and open spaces. Another example is that of a human-assisted UAV that operates in an unpredictable environment with a chance of having degraded or denied GPS signal, such as when inside an affected building or under bad weather conditions. This work aims to improve flight operation by providing reasonable and robust trajectory environment transitions.

The outline of this paper is as follows: multi-sensor fusion is described for estimation of 3D position, velocity, attitude, etc.; method of GPS measurement quality quantization is then presented; pre-scale process of SLAM is subsequently discussed; state estimation technique for UAV positioning during outdoor-to-indoor transition is then proposed following the experimental setup and field test results.

## 2. Multi-sensor fusion

Multi-sensor fusion (MSF) is a signal processing technique to combine information from different sensors with an aim to provide robust and complete navigation information for UAV localization. IEKF is one of the widely used multi-sensor fusions chosen for this work because its error-state guarantees Jacobian linearization, which is valid when operating close to the origin. Moreover, some second-order terms of the error-state could be neglected in the computation (Sola 2015).

### 2.1. IEKF

The IEKF categorizes state variables into two parts. They are the error-states ( $\tilde{\mathbf{x}}$ ), which are the small change of states in a short period of time, and the estimated-states ( $\hat{\mathbf{x}}$ ), which estimated the states from the last prediction. The true-state ( $\mathbf{x}$ ) is the suitable combination of error- and estimated-states, which is used as control feedback states in the control system.

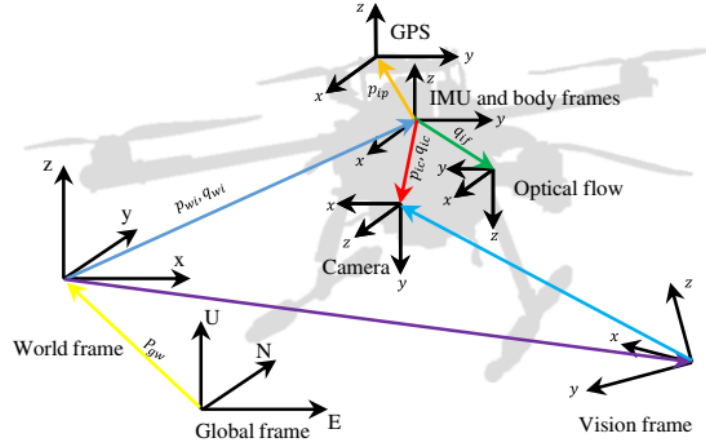
In this study, the MSF true-state of the UAV consists of 28 state variables, among which a six-degree-of-freedom position is included. The six-degree-of-freedom position consists of 10 states (three states of position, four states of orientation in quaternion, and three states of velocity to describe dynamic of the vehicle). The orientation is presented in quaternion to avoid the problem of gimbal lock phenomenon occurring at Euler angles. The remaining 18 states are auxiliary states for self-calibration of the UAV. The true-state is defined as

$$(1) \quad \mathbf{x}_t = \left\{ \mathbf{p}_{wi}^T \quad \mathbf{v}_{wi}^T \quad \mathbf{q}_{wi}^T \quad \mathbf{b}_\omega^T \quad \mathbf{b}_a^T \quad \lambda \quad \mathbf{p}_{wv}^T \quad \mathbf{q}_{if}^T \quad tz \quad \mathbf{p}_{ip}^T \right\}^T$$

where  $\mathbf{p}_{wi}$ ,  $\mathbf{v}_{wi}$ , and  $\mathbf{q}_{wi}$  are the position, velocity, and orientation state variables, respectively, expressed in the world frame;  $\mathbf{b}_\omega$  and  $\mathbf{b}_a$  are the gyroscope and accelerometer bias variables, respectively, expressed in the IMU frame;  $\lambda$  is the visual scale;  $\mathbf{p}_{wv}$  is the position of vision frame expressed in the world frame;  $\mathbf{q}_{if}$  is the quaternion rotational offset of the optical flow sensor frame relative to the IMU frame expressed in terms of the IMU frame;  $tz$  is the terrain height expressed in the world frame; and  $\mathbf{p}_{ip}$  is the position offset of the GPS sensor frame relative to the IMU frame written in terms of the IMU frame.

It is assumed that the IMU frame and the body frame are at the same place, as shown in Fig. 1. The world frame is the reference of the IEKF, which drifted over time.

Fig. 1. The UAV reference frames.



The stationary global frame is placed at the UAV takeoff point, which needed GPS to estimate the location. The result of the world frame drifted away from the global frame can be calculated by an estimator, and the difference is the takeoff point correction relative to the world frame in the control system. The camera frame is placed at the camera sensor lens and measured relative to the vision frame of the SLAM system. The vision frame is located where the SLAM system is initialized and usually not the same as the takeoff location.

Matrices and vectors are written in boldface while scalar values are written in italic type. The error-state of a UAV can be written as

$$(2) \tilde{\mathbf{x}} = \left\{ \delta \mathbf{p}_{wi}^T, \delta \mathbf{v}_{wi}^T, \delta \theta_{wi}^T, \delta \mathbf{b}_w^T, \delta \mathbf{b}_a^T, \delta \lambda, \delta \mathbf{p}_{wv}^T, \delta \theta_{if}^T, \delta tz, \delta \mathbf{p}_{ip}^T \right\}^T$$

where the error-state is defined as  $\delta \mathbf{x} = \mathbf{x}_t - \hat{\mathbf{x}}$  for position, velocity, and bias. The quaternion error-state is defined as the multiplication  $\delta \mathbf{q} = \mathbf{q} \otimes \hat{\mathbf{q}}^* \approx [(1/2)\delta \boldsymbol{\theta} \quad 1]^T$  as presented by Crassidis et al. (2007);  $\hat{[\cdot]}$  notation is for the estimated-state.

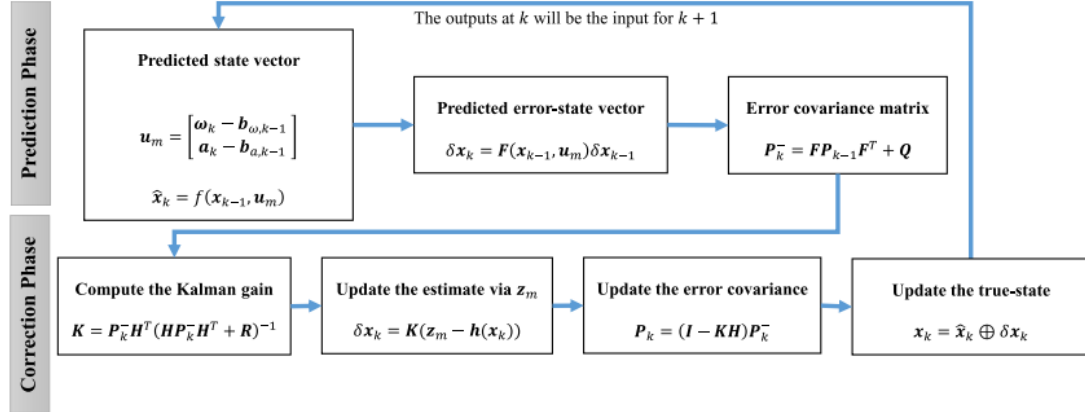
In this study, the multi-sensor fusion algorithm is developed based on the IEKF. It consists of two processing phases, as shown in Fig. 2. First, in the prediction phase, the IMU information (angular velocity  $\boldsymbol{\omega}$  and linear acceleration  $\mathbf{a}$ ) is treated as the control variable  $\mathbf{u}_m$  to propagate the estimated-state  $\hat{\mathbf{x}}_k$  by using the previous true-state of the system dynamic  $f(\mathbf{x}_{k-1}, \mathbf{u}_m)$ . Next, the discretized error-state system dynamic propagates the error-state  $\delta \mathbf{x}_k$  in the predicted error-state. Then, the estimated error covariance  $\mathbf{P}^-$  is determined by the error-state and discretized covariance matrix  $\mathbf{Q}$ . Second, the correction phase begins as soon as a sensor measurement  $\mathbf{z}_m$  is available. However, update rate of the correction phase is much slower than that of the prediction phase. The sensor measurement model  $\mathbf{h}(\mathbf{x})$  is linearized to be  $\mathbf{H}$  before computation of the Kalman gain  $\mathbf{K}$  that related to the sensor measurement covariance  $\mathbf{R}$ . Later, the Kalman gain is used to update the error state and error covariance. Consequently, the error-state is used for correction of the true-state that is then used in the next iteration.

## 2.2. Measurement of sensors

### 2.2.1. GPS measurement

For outdoor environment, GPS plays a major role in the world position measurement and also can be used to determine yaw measurement (Lynen et al. 2013). The yaw

Fig. 2. The multi-sensor fusion algorithm state diagram.



measurement is not directly provided by a GPS sensor. However, it can be determined by the UAV movement whereas the GPS sensor location relative to the IMU frame is known. For example, when the UAV purely rotates around the IMU frame, the GPS measurement and angular velocity change while the linear acceleration does not change. Thus, the prediction phase will report the UAV rotation movement. When the predicted GPS measurement is non-zero, the yaw measurement is corrected in every iteration in the correction phase. A 3D GPS position measurement model  $z_{\text{gps}}$  can be written as

$$(3) \quad z_{\text{gps}} = p_{\text{wi}} + C_{\text{wi}}^T p_{\text{ip}} + n_{\text{gps}}$$

where  $C_{\text{wi}} \triangleq C_{\text{wi}}(\hat{q}_{\text{wi}})$  is the quaternion-derived rotation matrix of the IMU frame with respect to the world frame and  $n_{\text{gps}}$  is the white Gaussian noise.

The error-state measurement is the difference between the true-state and the estimated-state, thus

$$(4) \quad \tilde{z}_{\text{gps}} = z_{\text{gps}} - (\hat{p}_{\text{wi}} + \hat{C}_{\text{wi}}^T \hat{p}_{\text{ip}})$$

where  $\tilde{z}_{\text{gps}}$  is the error-state of the 3D GPS position measurement and  $\hat{C}_{\text{wi}} \triangleq C(\hat{q}_{\text{wi}})$  is the rotation matrix corresponding to the estimated attitude  $\hat{q}_{\text{wi}}$ .

Equation (4) can be linearized as  $\tilde{z}_{\text{gps}} = H_{\text{gps}} \tilde{x}$  where Jacobian  $H_{\text{gps}}$  denotes the Jacobian of GPS measurement with respect to the error-state, thus

$$(5) \quad H_{\text{gps}} = \begin{bmatrix} \mathbf{I}_{3 \times 3} & \mathbf{0}_{3 \times 3} & -\hat{C}_{\text{wi}}[\hat{p}_{\text{ip}}]_{\times} & \mathbf{0}_{3 \times 14} & \hat{C}_{\text{wi}} \end{bmatrix}$$

where  $[\cdot]_{\times}$  is the skew matrix.

The  $-\hat{C}_{\text{wi}}[\hat{p}_{\text{ip}}]_{\times}$  term can be used to recover the attitude error-state  $\delta\theta_{\text{wi}}$  of  $\tilde{x}$ . That is, the position measurement can be used as the attitude error measurement as long as the offset position between the GPS sensor and IMU sensor  $\hat{p}_{\text{ip}}$  is non-zero. The observability analysis has guaranteed that the yaw measurement is observable (Weiss 2012). Covariance of GPS measurements can be obtained directly from the GPS module because horizontal accuracy estimate is available. Covariance of the GPS measurement — an indicator of the UAV environment whether it is indoor or outdoor — increases when satellite signal is obstructed. This will be further discussed in Sect. 3.

### 2.2.2. Vision measurement

In this work, the ORB-SLAM-Inertial software package provides a six-degree-of-freedom measurement of position and orientation. The obtained map and graph-based optimization provide a better measurement than the GPS does. The ORB-SLAM-Inertial uses FAST corner and ORB descriptor to estimate the camera pose, and applies bundle adjustment to refine the map points as shown in Fig. 3. On the other hand, the IMU data is used to calculate the scale using the pre-integration technique as discussed in Sect. 4. Then, the scaled camera pose is corrected by an initial offset, which is the alignment of the vision measurement to the current state of the IEKF, as mentioned in Sect. 5. In the IEKF measurement, the vision is finally measured relative to the vision frame as soon as the SLAM is initialized.

This work proposes the vision measurement model, which estimates the position drift of the vision frame away from the world frame expressed in terms of the world frame, and the drift scale to work with low-cost sensor and processor. Other states, such as position and orientation offsets between the camera and IMU frames are calibrated offline using Kalibr toolbox (Maye et al. 2013). The 3D position vision measurement model  $z_{v,p}$  can be defined thus

$$(6) \quad z_{v,p} = (\mathbf{p}_{wi} - \mathbf{p}_{wv})\lambda + \mathbf{n}_p$$

The error measurement can be defined as

$$(7) \quad \tilde{z}_{v,p} = z_{v,p} - (\hat{\mathbf{p}}_{wi} - \hat{\mathbf{p}}_{wv})\hat{\lambda}$$

which can be linearized as  $\tilde{z}_{v,p} = \mathbf{H}_{v,p}\tilde{\mathbf{x}}$ , where the Jacobian  $\mathbf{H}_{v,p}$  is

$$(8) \quad \mathbf{H}_{v,p} = \begin{bmatrix} \mathbf{I}_{3 \times 3}\hat{\lambda} & \mathbf{0}_{3 \times 12} & (\hat{\mathbf{p}} - \hat{\mathbf{p}}_{wv})^T & \mathbf{I}_{3 \times 3}\hat{\lambda} & \mathbf{0}_{3 \times 7} \end{bmatrix}$$

The vision attitude measurement  $z_m$  is calculated by

$$(9) \quad z_m = \mathbf{q}_{wv} \otimes \mathbf{q}_{vc,m} \otimes \mathbf{q}_{ic}^*$$

where  $\mathbf{q}_{wv}$  is the attitude offset of the vision frame with respect to the world frame,  $\mathbf{q}_{w,m}$  is the attitude measurement from SLAM system, and  $\mathbf{q}_{ic}$  is the attitude of camera frame with respect to the IMU frame. Both  $\mathbf{q}_{wv}$  and  $\mathbf{q}_{ic}$  are constants and will be analyzed in Sects. 5 and 6, respectively. Hence, the attitude measurement model  $z_{v,q}$  can be written as

$$(10) \quad z_{v,q} = \mathbf{q}_{wi} \otimes \mathbf{q}_n$$

where  $\mathbf{q}_n$  is the attitude zero-mean white Gaussian noise.

The attitude error measurement can be written as

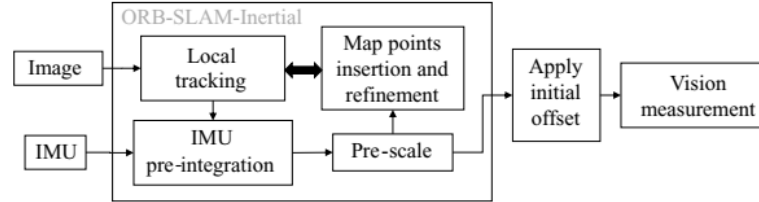
$$(11) \quad \tilde{z}_{v,q} = z_q - \hat{z}_q = \mathbf{q}_{wi} \otimes (\hat{\mathbf{q}}_{wi})^{-1}$$

Error measurement of the attitude can be linearized as  $\tilde{z}_{v,q} = \mathbf{H}_{v,q}\tilde{\mathbf{x}}$  where the Jacobian  $\mathbf{H}_{v,q}$  denotes the Jacobian of vision attitude measurement with respect to the error-state

$$(12) \quad \mathbf{H}_{v,q} = \begin{bmatrix} \mathbf{0}_{3 \times 6} & \mathbf{I}_{3 \times 3} & \mathbf{0}_{3 \times 17} \end{bmatrix}^T$$

In general, vision measurements have some time delay compared to IMU measurements. This means that the images taken display disagreeing timestamps because of ambient light change between indoor and outdoor flight, for example (Hutchison et al. 2010).

Fig. 3. The vision measurement flowchart.



The unsynchronized measurement can affect both the accelerometer and the gyroscope bias estimations. Optimal time of adjustment is needed to correct the timestamp between the image trigger and the IMU measurement. This can be calculated offline using least-square optimization, thus

$$(13) \quad t_{\text{delay}} = dt \min_d \left( \sum_{k=1}^N \|z_{q,k} - \hat{q}_{wi,k-d}\| \right)$$

where  $t_{\text{delay}}$  and  $dt$  are the optimal time delay and the sample period, respectively;  $z_{q,k}$  and  $\hat{q}_{wi,k-d}$  are the visual orientation measurement and the  $d$ th prior iteration of the estimated orientation from MSF. Position measurement is not used in this step because the position can be scaled arbitrarily. Sufficient rotational excitation for all axes is required to correct the measurement (Yang and Shen 2017).

The quality of visual SLAM measurement would be low with a lot of outliers when operated under outdoor environment due to the more distant scene (Hutchison et al. 2010). Thus, a fuzzy logic rule table is applied to classify the priority between visual SLAM and GPS measurement, thus,

$$(14) \quad \sigma_{v,p} = 2\sigma_{v,p} \frac{\sigma_{\text{gps}}^*}{\sigma_{\text{gps}}}$$

where  $\sigma_{v,p}$  is the artificial variance of vision positioning; and  $\sigma_{\text{gps}}$  and  $\sigma_{\text{gps}}^*$  are the GPS horizontal variance and its cutoff level, respectively.

### 2.2.3. Barometer measurement

In practice, GPS height estimation fluctuates widely at low altitude (Shi and Cannon 1995). Therefore, a barometer is used to measure the altitude, especially when operating under outdoor environment. The barometer measurement model can be written as

$$(15) \quad z_{pz} = p_{wi,z} + n_{pz}$$

where  $p_{wi,z}$  is the height (in the  $z$ -direction) of the position state  $p_{wi}$  expressed in terms of the world frame and  $n_{pz}$  is the white Gaussian noise.

The error measurement of barometer can be written as

$$(16) \quad \tilde{z}_{pz} = z_{pz} - \hat{p}_{wi,z}$$

where  $\hat{p}_{wi,z}$  is the estimated height (in the  $z$ -direction) of the position state  $p_{wi}$  expressed in terms of the world frame.

The error measurement of barometer can be linearized as  $\tilde{z}_{pz,1} = H_{pz} \tilde{x}$  where the Jacobian  $H_{pz}$  can be defined as



$$(17) \mathbf{H}_{pz} = \begin{bmatrix} \mathbf{0}_{1 \times 2} & 1 & \mathbf{0}_{1 \times 23} \end{bmatrix}$$

#### 2.2.4. Optical flow measurement

When an UAV has only vision measurement data (GPS measurement is denied), the position scale estimation calculated based on vision, barometric, and IMU measurement may not be enough in some cases, such as when flying with a constant height and velocity. This makes scale estimation prone to divergence, especially when the actual scale is largely different from the estimated scale.

Optical flow is chosen as the body velocity measurement to improve scale estimation and to prevent scale divergence. It is assumed that the UAV flies at low speed over a leveled terrain. The relationship between the mean displacement of the optical flow sensor and the angular velocity can be written thus

$$(18) \mathbf{v}_f = -\frac{h}{\Delta t} \mathbf{S}(\mathbf{v}_{\text{abs}} - \boldsymbol{\omega})$$

where  $h$  is the height above ground level (AGL) expressed in terms of the world frame, ( $h = p_{w_i,z} - tz$ , calculated from the previous state);  $\Delta t$  is the flow sampling period;

$$\mathbf{S} = \begin{bmatrix} 1 & 0 & 0 \\ 0 & 1 & 0 \end{bmatrix}$$

is the selective matrix that allows the pixel displacement to be expressed only in the  $x$ - and  $y$ -axes;  $\mathbf{v}_{\text{abs}} \in \mathbb{R}^{3 \times 1}$  is the pixel displacement per metre in the  $x$ - and  $y$ -axes of the body frame; and  $\boldsymbol{\omega}$  is the body angular velocity from the optical flow internal gyroscope.

The optical flow measurement model  $\mathbf{z}_f$  can be written as

$$(19) \mathbf{z}_f = \mathbf{S} \mathbf{C}_{\text{if}}^T \mathbf{C}_{w_i}^T \mathbf{v}_{w_i} + \mathbf{n}_f$$

where  $\mathbf{C}_{\text{if}} \triangleq \mathbf{C}_{\text{if}}(\mathbf{q}_{\text{if}})$  is the rotation matrix of the optical flow sensor relative to the IMU frame expressed in terms of the IMU frame and  $\mathbf{n}_f$  is the white Gaussian noise.

The error measurement model is

$$(20) \tilde{\mathbf{z}}_f = \mathbf{z}_f - \mathbf{S} \hat{\mathbf{C}}_{\text{if}}^T \hat{\mathbf{C}}_{w_i}^T \hat{\mathbf{v}}_{w_i}$$

This can be linearized to  $\tilde{\mathbf{z}}_f = \mathbf{H}_f \tilde{\mathbf{x}}$  using the relation  $\mathbf{C}_{w_i}^T \approx (\mathbf{I} - [\delta \boldsymbol{\theta}_{w_i}]_{\times}) \hat{\mathbf{C}}_{w_i}^T$  and the skew matrix property  $[\mathbf{a}]_{\times} \mathbf{b} = -[\mathbf{b}]_{\times} \mathbf{a}$ .

The Jacobian  $\mathbf{H}_f$  can be written as

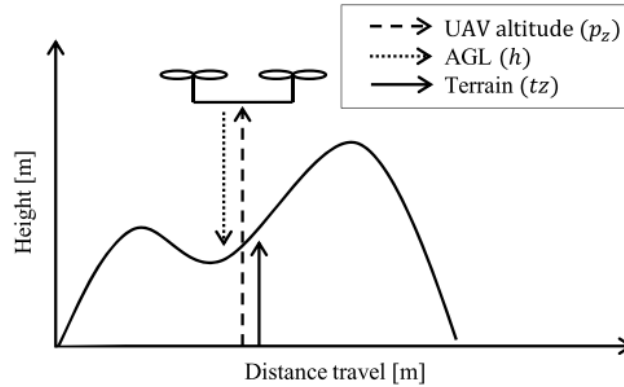
$$(21) \mathbf{H}_f = \begin{bmatrix} \mathbf{0}_{2 \times 3} & \mathbf{S} \hat{\mathbf{C}}_{\text{if}}^T \hat{\mathbf{C}}_{w_i}^T & \mathbf{S} \hat{\mathbf{C}}_{\text{if}}^T \left[ \hat{\mathbf{C}}_{w_i}^T \hat{\mathbf{v}}_{w_i} \right]_{\times} & \mathbf{0}_{2 \times 10} & \mathbf{S} \left[ \hat{\mathbf{C}}_{\text{if}}^T \hat{\mathbf{C}}_{w_i}^T \hat{\mathbf{v}}_{w_i} \right]_{\times} & \mathbf{0}_{2 \times 4} \end{bmatrix}$$

Visual scale  $\hat{\lambda}$  is always observable by the body velocity measurement (Weiss 2012).

#### 2.2.5. Terrain measurement

To achieve accurate body velocity estimation from the optical flow sensor, the AGL measurement and its estimation must be accurate as well. Low-cost ultrasonic sensors often give faulty measurements over outdoor terrain, for example, when measuring over grass or rough floor, and in noisy environment. Instead of direct estimation, ultrasonic sensing information of the ground level is estimated using MSF, and then the AGL is used to determine the terrain height, as shown in Fig. 4.

**Fig. 4.** Relationship between terrain height, above-ground level (AGL), and estimated UAV altitude from the barometer.



The terrain measurement model can be defined as

$$(22) \quad z_{tz} = p_{wi,z} - tz + n_{tz}$$

where  $p_{wi,z}$  is the height (z-axis) of the IMU frame with respect to the world frame;  $tz$  is the terrain height; and  $n_{tz}$  is the white Gaussian noise.

The error measurement model can be defined as

$$(23) \quad \tilde{z}_{tz} = z_{tz} - (\hat{p}_{wi,z} - \hat{tz})$$

which can be linearized as  $\tilde{z}_{tz} = \mathbf{H}_{tz} \tilde{\mathbf{x}}$  where the Jacobian  $\mathbf{H}_{tz}$  can be written as

$$(24) \quad \mathbf{H}_{tz} = [\mathbf{0}_{1 \times 2} \quad 1 \quad \mathbf{0}_{1 \times 19} \quad -1 \quad \mathbf{0}_{1 \times 3}]$$

The Mahalanobis distance is used to reject outlier of the terrain measurement when the outlier is larger than the critical  $\chi^2$ .

Finally, the AGL can be computed by  $\hat{h} = \hat{p}_{wi,z} - \hat{tz}$  for scaling up the optical flow velocity to the next iteration.

### 3. GPS quality indicator

GPS measurement should be taken into account only when its variance is less than a specific value. Many studies rely on pseudo-range (Serranoa et al. 2014) or horizontal-vertical dilution of precision (HDOP-VDOP) (Kealy et al. 2010) to qualify the GPS signal. In practice, pseudo-range algorithm is complex, but on the other hand, the HDOP-VDOP cutoff method is too slow and too rough to be implemented on highly dynamic UAV state estimation. Recently, GPS horizontal-vertical position accuracy (hAcc-vAcc), which corresponds to  $1\sigma$  value in metric units, is successfully used as GPS position measurement variance in many commercial UAV firmware (e.g., PX4 and Ardupilot) (Meier et al. 2015; ArduPilot Open Source Autopilot) with advantages such as fast response, high accuracy, and the ability to be implemented on low-cost GPS sensors.

Nevertheless, hAcc-vAcc variance provides a poor estimation when the number of visible satellites is  $<5$ . This is because hAcc-vAcc variance increases slowly and is not suitable for being used as a cutoff number. This happens when the UAV flies close to a tall building and the GPS sensor yields faulty position measurements before the state-estimations switch

off the GPS information, and this fault indicates wrongly that it is indoors. To avoid this problem, this work proposes a method to indicate GPS quality using gradient of the GPS variance.

The gradient of hAcc variance is defined as

$$(25) \quad \Delta\sigma = \sigma_k - \sigma_{k-1}$$

$$(26) \quad \sigma_{\text{bounded}} = \sigma_{\text{min}} \leq \sigma_k \leq \sigma_{\text{max}}$$

where  $\Delta\sigma$  is the gradient of the variance and  $\sigma_k$  is the hAcc variance information from the GPS sensor at the  $k$ th iteration.

The qualified variables as the criteria function  $D(\sigma)$  can be defined as

$$(27) \quad D(\sigma_{\text{bounded}}) = \text{sgn}(\Delta\sigma) \left[ \text{sgn}(\Delta\sigma)(\beta - 1) \left( \frac{\sigma_{\text{bounded}} - \sigma_{\text{min}}}{\sigma_{\text{max}} - \sigma_{\text{min}}} \right) + B \right]$$

where  $\text{sgn}(\cdot)$  is the sign function that extracts the sign of a real number and

$$B = \begin{cases} 1 & \text{when } \Delta\sigma > 0 \\ \beta & \text{when } \Delta\sigma < 0 \end{cases}$$

where  $\beta$  is the selected response rate where  $0 < \beta < 1$ .

Figure 5 shows the behavior output from the criteria function eq. (27) when the GPS variance changes. For example, a UAV has a current GPS variance of 3 m outdoors, then the UAV goes indoors, the variance increases to 4 m ( $\Delta\sigma > 0$ ), so the criterion of the bad trend line (the upper dashed line in Fig. 5) is used to calculate the quality score, which is from Point 1 to Point 2. When the UAV comes back outdoors, the GPS variance reduces from 4 to 2.5 m ( $\Delta\sigma < 0$ ), the criterion is calculated along the good GPS trend line (the lower full-line) from Point 3 to Point 4.

The criteria values of good and bad trends are determined as soon as the GPS variance changes direction ( $\Delta\sigma$  sign is changed). Whenever the UAV goes indoors again, the GPS variance increases ( $\Delta\sigma > 0$ ) and the criteria function will switch back to the bad trend line again (Point 4 to Point 5). These criteria values are always updated and used to determine the GPS quality indicator score for turning on or turning off the GPS measurement,

$$(28) \quad \text{score}_k = \begin{cases} \text{score}_{k-1} + D & \text{when } \Delta\sigma \neq 0 \\ \text{score}_{k-1} + \text{sgn}(\Delta\sigma_d)\beta & \text{when } \Delta\sigma = 0 \end{cases}$$

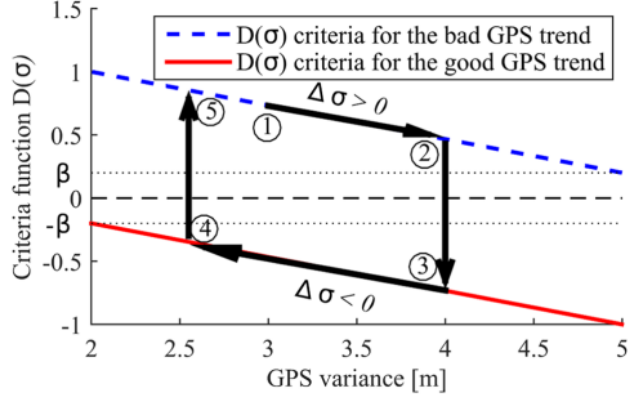
where  $\text{score}_k$  is the  $k$ th iteration of the GPS measurement where  $\text{score}_{\text{min}} \leq \text{score}_k \leq \text{score}_{\text{max}}$  and  $\Delta\sigma_d$  is the last non-zero GPS gradient at the  $d$ th iteration.

If there is no change of the GPS variance ( $\Delta\sigma = 0$ ), the GPS indicator score would still be updated by the  $\beta$  bias. The score is to indicate whether the UAV is indoors or outdoors, and to turn off the GPS measurement when it is indoors (high positive score). However, the GPS variance would still be calculated to be ready to turn on the GPS measurement when it is outdoors (high negative score).

#### 4. Pre-scale process in vision measurement

Large discrepancy between an initial guess scale and a real scale causes unstable state estimation (Weiss 2012). An initial guess scale is determined before feeding to the estimator. The initial guess scale is estimated using IMU pre-integration technique (Forster et al. 2017), which summarizes hundreds of IMU measurement data into one single

**Fig. 5.** Criteria function  $D(\sigma)$  for increasing GPS variance (the upper dashed line, when  $\Delta\sigma > 0$ ) and decreasing GPS variance (the lower solid line, when  $\Delta\sigma < 0$ ).



measurement. Position, velocity, and attitude measurements are used for short-term scaling of the SLAM until a new vision keyframe is available.

The IMU pre-integration form had been presented by [Mur-Artal and Tardós \(2017\)](#). Accelerometer measurement  $\mathbf{a}_m$  and gyroscope measurement  $\omega_m$  are used to calculate the position ( $\mathbf{p}_{vi}$ ), velocity ( $\mathbf{v}_{vi}$ ), and attitude ( $\mathbf{C}_{vi}$ ) of the IMU frame with respect to the vision frame written in terms of the vision frame. These measurements can be discretized for the  $k$ th to the  $(k+1)$ th iteration thus

$$(29) \quad \mathbf{p}_{vi}^{k+1} = \mathbf{p}_{vi}^k + \mathbf{v}_{vi}^k \Delta t + \frac{1}{2} \mathbf{g} \Delta t^2 + \frac{1}{2} \mathbf{C}_{vi}^k (\mathbf{a}_m^k - \mathbf{b}_a^k) \Delta t^2$$

$$(30) \quad \mathbf{v}_{vi}^{k+1} = \mathbf{v}_{vi}^k + \mathbf{g} \Delta t + \mathbf{C}_{vi}^k (\mathbf{a}_m^k - \mathbf{b}_a^k) \Delta t$$

$$(31) \quad \mathbf{C}_{vi}^{k+1} = \mathbf{C}_{vi}^k \exp[(\omega_m^k - \mathbf{b}_\omega^k) \Delta t]$$

where  $\omega_m$  and  $\mathbf{a}_m$  are the angular velocity and the linear acceleration measurements from the IMU sensor;  $\mathbf{b}_a$  and  $\mathbf{b}_\omega$  are the accelerometer and gyroscope biases, respectively, obtained from MSF since the initial guess became available;  $\exp(\cdot)$  is the *exponential map* that can be estimated as the first-order approximation of  $\exp(\phi_\times) \approx \mathbf{I} + \phi_\times$ , where  $\phi$  is the  $\mathbb{R}^3$  vector; and  $\mathbf{g}$  is the gravity vector.

In between the vision keyframes  $i$  and  $i+1$ , the position, velocity, and attitude measurements can be summarized as  $\Delta \mathbf{p}_{vi}^{i,i+1}$ ,  $\Delta \mathbf{v}_{vi}^{i,i+1}$ , and  $\Delta \mathbf{C}_{vi}^{i,i+1}$ , respectively. Thus, the IMU pre-integration can be determined as

$$(32) \quad \mathbf{p}_{vi}^{i+1} = \mathbf{p}_{vi}^i + \mathbf{v}_{vi}^i \Delta T + \frac{1}{2} \mathbf{g} \Delta T^2 + \mathbf{C}_{vi}^i (\Delta \mathbf{p}_{vi}^{i,i+1} + \mathbf{J}_{\Delta p}^\omega \mathbf{b}_\omega^i + \mathbf{J}_{\Delta p}^a \mathbf{b}_a^i)$$

$$(33) \quad \mathbf{v}_{vi}^{i+1} = \mathbf{v}_{vi}^i + \mathbf{g} \Delta T + \mathbf{C}_{vi}^i (\Delta \mathbf{v}_{vi}^{i,i+1} + \mathbf{J}_{\Delta v}^\omega \mathbf{b}_\omega^i + \mathbf{J}_{\Delta v}^a \mathbf{b}_a^i)$$

$$(34) \quad \mathbf{C}_{vi}^{i+1} = \mathbf{C}_{vi}^i \Delta \mathbf{C}_{vi}^{i,i+1} \exp(\mathbf{J}_{\Delta C} \mathbf{b}_\omega^i)$$

where  $\Delta T$  is the time difference between two consecutive keyframes  $i$  and  $i+1$ ; and  $\mathbf{J}_{(\cdot)}^\omega$  and  $\mathbf{J}_{(\cdot)}^a$  are the Jacobians of changing bias calculated ([Forster et al. 2017](#)).

The relationship of the estimated IMU measurement and the estimated SLAM in between any two consecutive keyframes is

$$(35) \quad \mathbf{p}_{vi} = s\mathbf{p}_{vc} + \mathbf{C}_{vc}\mathbf{p}_{ci}$$

where  $\mathbf{p}_{vi}$  is the IMU position estimated by eq. (32);  $s$  is the scale of the camera trajectory corresponding to the world frame;  $\mathbf{p}_{vc}$  is the camera position estimated by the SLAM system; and  $\mathbf{p}_{ci}$  is the IMU frame with respect to the camera frame.

After the initial guess of the gyroscope bias is obtained by MSF, the scale and gravity vectors are determined using singular value decomposition of at least four consecutive keyframes (Mur-Artal and Tardós 2017). The gyroscope and accelerometer biases are also refined during the scale initialization process. Finally, the estimated scale is used for mapping points on any prior keyframes within the SLAM system.

## 5. Seamless transition position measurement

When a new type of position measurement emerges, consistency between the new position sensor measurement and the current estimated position must be properly handled before feeding into the MSF as measurement for the next state estimation, otherwise it may cause an unnecessary skip trajectory as shown in Fig. 6a. The difference between the new sensor position measurement (star) and the estimated-state (dashed line) causes an interrupting change of the next position estimation, and that leads the UAV to fly in the opposite direction to the offset direction to maintain its previous desired trajectory. This can be improved by offsetting the estimated-state.

However, it is not straightforward to apply the offset due to sensor measurement noise. The graph-based optimization method proposed by Shen et al. (2014) used a laser, vision-based odometry, and GPS information to smooth the offset. In this work, an alternative 3D position smoothing offset is proposed, that is, by applying a low-pass filter to reduce sensor measurement noise uncertainty. With the benefit of compact code and less computation load, the method gains smooth position offset using only one sensor. Offset between the position state  $\mathbf{p}_{wi}$  and the position measurement  $z_p$  can be written in the form of a low-pass filter as

$$(36) \quad \Delta\mathbf{P}_k = \Delta\mathbf{P}_{k-1}(1 - \alpha) + \alpha(\mathbf{P}_{wi} - \Delta\mathbf{P}_{k-1} - z_p)$$

where  $\Delta\mathbf{P}_k$  and  $\Delta\mathbf{P}_{k-1}$  are the smooth offsets of the current and the prior iterations, respectively and  $\alpha$  is the low-pass smoothing factor where  $0 < \alpha < 1$ , and can be calculated thus

$$(37) \quad \alpha = \frac{T_s}{RC + T_s}$$

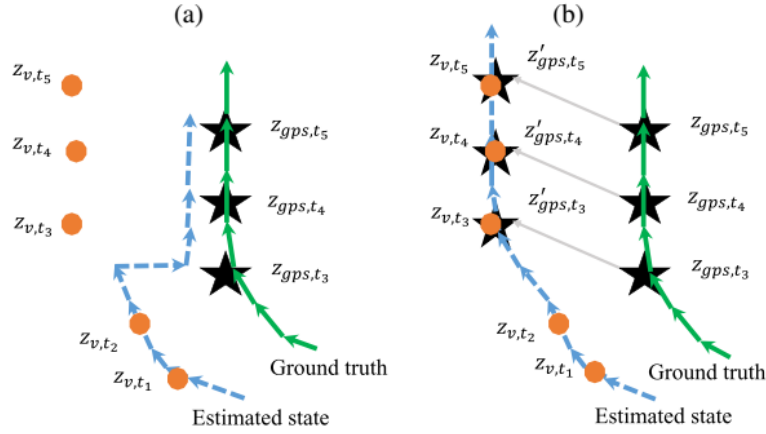
where  $T_s$  is the sensor measurement period and the sensor time constant  $RC \triangleq 1/2\pi f_c$ , where  $f_c$  is the cutoff frequency corresponding to the position measurement noise.

The new available sensor (GPS or vision-based) added to smooth the position offset  $\Delta\mathbf{P}_k$  leads to a smooth position measurement.

In general, the position offset  $\Delta\mathbf{P}_k$  may cause misalignment between the global frame and UAV world frame, especially when GPS sensor measurement is applied, for example, in the case of an UAV flying indoors to outdoors. The offset is due to accumulation in position drifts in the estimated vision position. This can be solved by shifting the home reference point by the same amount of  $\Delta\mathbf{P}_k$  in the UAV world frame. The shifted home reference point is the global frame reference.

For the vision measurement offset, the initial vision orientation frame offset must be calculated before applying the smooth position offset. In general, to have a proper scale of a monocular SLAM system, a UAV must travel for some time to ensure that all observable

**Fig. 6.** Estimated position behavior from different GPS position measurement  $z_{gps,t}$  and vision position measurement  $z_{v,t}$ , (a) without smoothing offset and (b) with smoothing offset.



parameters are sufficiently excited before calculating the initial vision frame (Mur-Artal and Tardós 2017).

The initial offset of the vision frame  $\mathbf{p}_{wv}$  and  $\mathbf{q}_{wv}$  with respect to the world frame can be calculated using the last  $d$ th iteration of the position  $\hat{\mathbf{p}}_{wi,k-d}$  and quaternion  $\hat{\mathbf{q}}_{wi,k-d}$  estimated-state where the  $k$ th is the current iteration of the vision measurement, thus

$$(38) \quad \mathbf{p}_{wv} = \hat{\mathbf{p}}_{wi,k-d} + \hat{\mathbf{q}}_{wi,k-d} \otimes \bar{\mathbf{p}}_{iv} \otimes \hat{\mathbf{q}}_{wi,k-d}^*$$

where

$$\bar{\mathbf{p}}_{iv} = \begin{bmatrix} \mathbf{p}_{iv} \\ 0 \end{bmatrix}$$

is the quaternion form of the position vision frame with respect to the IMU frame calculated using

$$(39) \quad \mathbf{p}_{iv} = \mathbf{p}_{ic} + \mathbf{q}_{ic}^* \otimes (-\bar{\mathbf{p}}_{vc}) \otimes \mathbf{q}_{ic}$$

and the orientation of vision frame  $\mathbf{q}_{wv}$  with respect to the world frame is determined using

$$(40) \quad \mathbf{q}_{wv} = \mathbf{q}_{wi,k-d} \otimes \mathbf{q}_{ic} \otimes \mathbf{q}_{vc}$$

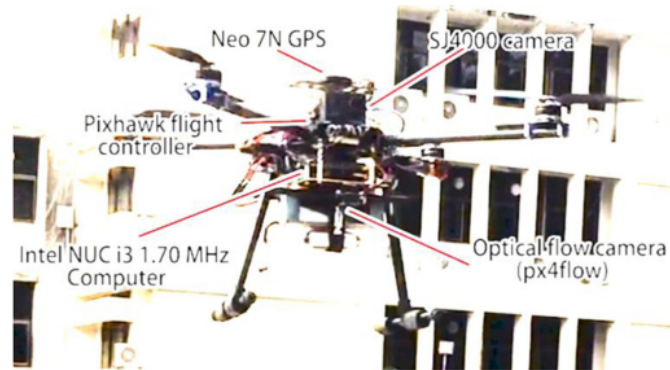
where  $\mathbf{p}_{ic}$  and  $\mathbf{q}_{ic}$  are the position and orientation offsets between the camera frame and the IMU frame that can be obtained from Kalibr toolbox (Maye et al. 2013);

$$\bar{\mathbf{p}}_{vc} = \begin{bmatrix} \mathbf{p}_{vc} \\ 0 \end{bmatrix}$$

is the camera position with respect to the vision frame; and  $\mathbf{q}_{vc}$  is the orientation of the camera frame with respect to the vision frame.

All discussed algorithms, especially the multi-sensor fusion scheme, need to identify sensing characteristic constants, such as noise densities, random walks, and measurement delays. These constants depend on a specific platform setup, to be discussed in Sect. 6.

Fig. 7. The tested UAV setup.



## 6. Implementation and setup

### 6.1. The UAV platform

The tested UAV is a quadrotor platform, as depicted in Fig. 7. The autopilot is developed based on PX4 firmware (Meier et al. 2015). The Pixhawk flight controller is originally equipped with an IMU 3-axis accelerometer + gyroscope (MPU6000), external compass (HMC5883L), barometric sensor (MS5611), external optical flow sensor (PX4FLOW), external GPS (Ublox NEO-7N), and a CMOS camera (SJ4000) as a visual SLAM monocular.

For state estimation, obstacle avoidance and trajectory generation are processed on an Intel NUC computer with i3-4010U Processor (3M Cache, 1.70 GHz), 128 GB SSD, and 4 GB memory. The computer is installed on the UAV. The total takeoff mass is 2.41 kg, including two LiPo batteries (4s 5000 mAh and 3s 1500 mAh). All presented algorithms are implemented and tested on this UAV platform.

### 6.2. Real-time onboard software

Our proposed algorithm, named “Crossover”, is developed in C++, which runs on an onboard computer with Robot Operating System (ROS) as a middleware. The workflow diagram is shown in Fig. 8. The Pixhawk flight controller communicates to the computer via a USB serial port with Mavlink (Meier et al. 2013) protocol. The SLAM node for vision positioning (ORB\_SLAM2) is modified by the pre-integration IMU technique (Forster et al. 2017) to calibrate the initial scale, as mentioned in Sect. 4. However, in this case the modified ORB\_SLAM2 is not continuously taking the IMU information into the bundle adjustment as (Mur-Artal and Tardós 2017) did. Hence, it reduces the computational burden but with a less long-term accuracy.

### 6.3. Control system

To optimize gains in low-level control system of the PX4 firmware, the PX4tools (Droncrew 2017) for PID optimal gains are used. For high-level control system, the linear model predictive control (MPC) proposed by Kamel et al. (2017) is implemented to create 3D flight trajectories. The second-order plant can be obtained from system identification to determine the optimal roll and pitch transfer functions for the plant model of MPC framework according to Sa et al. (2017).

### 6.4. Determination of system parameters

The Allan standard deviation is used for identification and measurement of noise and drift, as shown in Tables 1 and 2. In practice, we have found that the standard deviation

Fig. 8. Processing workflow diagram of the UAV system.

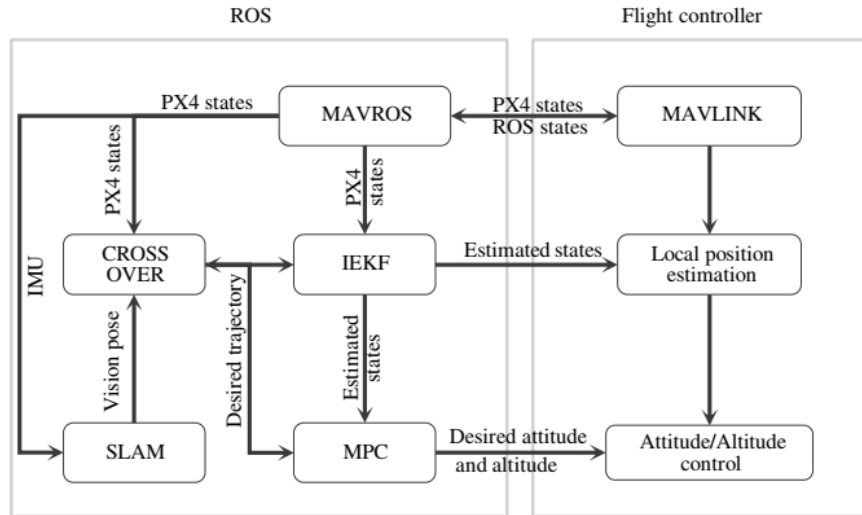


Table 1. Gyroscope and accelerometer random walks obtained from Allan standard deviation method of the IMU.

Parameter	Value
Gyroscope random walk	0.000195 rad/s <sup>2</sup> √Hz
Acc random walk	0.00904 m/s <sup>3</sup> √Hz

Table 2. Continuous-time accelerometer, gyroscope, and barometer measurement noises.

Parameter	Value
Acc XY noise density	0.090 m/s <sup>2</sup> √Hz
Acc Z noise density	0.198 m/s <sup>2</sup> √Hz
Gyroscope noise density	0.01380 rad/s√Hz
Barometer noise density	0.0788 m/√Hz

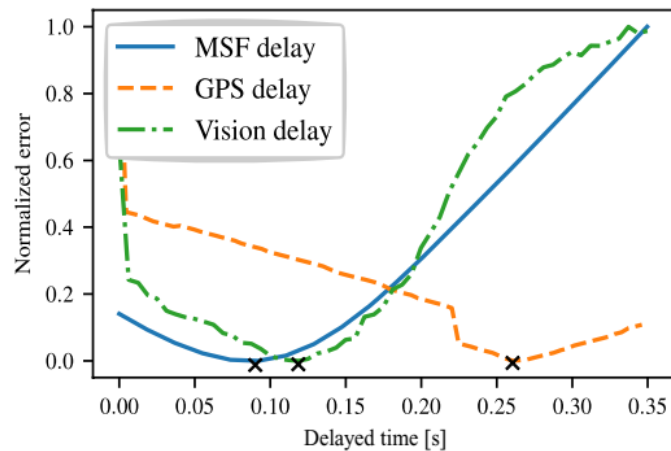
values of low-cost sensors often need to be multiplied by 10 or more to cover vibration effect during the flight.

In practice, timestamps of individual sensor’s measurement are not synchronized and are typically affected by a delay, which reduces the performance of the state estimation in terms of speed estimation and accuracy. The delay time in communication between the flight controller and the ROS message is caused by several reasons (e.g., USB latency) (Meier et al. 2012). This is computed using least-squared optimization in eq. (13). Results of the time delay of each measurement compared with the IMU timestamp, except the MSF delay, which is compared to the flight controller system timestamp, are shown in Table 3. Figure 9 shows a plot of normalized errors related to the time delay. The × marked points



**Table 3.** Delay of MSF-to-Pixhawk, GPS, and vision measurements.

Parameter	Time (s)
MSF to Pixhawk delay	0.092
GPS delay	0.265
Vision measurement delay	0.119

**Fig. 9.** Optimal measurement delay calculated using least-square optimization.

are the optimal delayed time of each measurement. The MSF delay time also occurs due to the latency of data transfers. The MSF state is estimated as a measurement of the low-level IEKF inside the flight control computation to compensate for the delay.

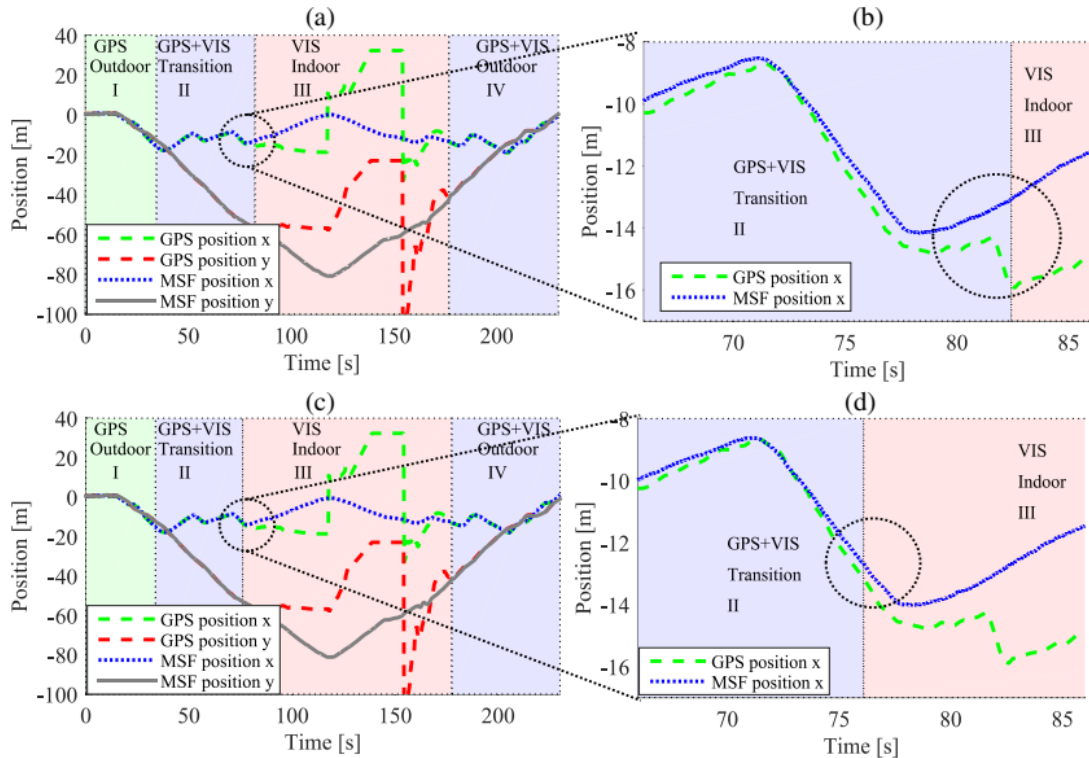
## 7. Experimental results

Because this work is to design a smooth navigation system during transition between outdoor and indoor flight, the test emphasizes the UAV state in the transition period. To show the algorithm performance, the UAV is tested over a large open space and the result obtained from the proposed algorithms is compared with the conventional GPS-based cutoff algorithm. The test field encompasses an eight-storey building and another 10 m tall building to ascertain that GPS signals would diminish when the UAV is close to the buildings.

Figures 10a and 10b show the MSF estimated position and the GPS position plotted using conventional GPS-based cutoff algorithm. The bottom row is the MSF estimated position which is plotted using the proposed GPS quality indicator algorithm. The marked background regions are labeled as the sensor transition state as follows: the first state (I), when GPS is available but vision SLAM is not available or in pre-scale processing; the second state (II), when both GPS and vision SLAM are available; the third state (III), when GPS is not available while vision SLAM is available; and the fourth state (IV), when GPS is regained and vision is available.

In the case of outdoor-to-indoor transition, the enlarged plots are shown in Figs. 10b and 10d. Figure 10b shows that position estimation with GPS-based cutoff takes more time to indicate that GPS is worse than that of position estimation with the GPS quality indicator

**Fig. 10.** MSF estimated position with the GPS-based cutoff (a and b), and with the proposed GPS quality indicator algorithm (c and d).



algorithm in Fig. 10d. Thus, the proposed GPS quality indicator algorithm can reasonably reject the GPS measurement before the false trajectory from the GPS measurement gets too far off. Furthermore, when the system quickly rejects the false GPS measurement, it means that the UAV will have better agility handling during the transition.

In the case of indoor-to-outdoor transition, the zoom plots are shown in Figs. 11b and 11d. The MSF estimated position without the proposed smoothing shown in Fig. 11b jumps to a GPS position with a difference of more than 2 m. This large jump is due to the fact that the estimated position carries position error over time from vision SLAM. This large offset can affect the UAV flight because the UAV will try to maintain its previous desired trajectory, and that leads the UAV to fly in the opposite direction to the offset direction to reduce the position error.

On the other hand, the proposed algorithm shown in Fig. 11d can better smooth the path between the GPS position and MSF estimated position by applying the offset to the GPS measurement to reduce the difference between them and provide a more reasonable trajectory for MSF estimation.

The position and velocity covariances generated from the MSF estimated position during the flight are shown in Fig. 12. The result shows that the covariances continuously increase when there is no GPS signal during the indoor flight (State III), and the covariances decrease and converge to a certain value when flying toward the outdoors.

The position covariance is divergent when GPS is not available, but the velocity covariance stays in bound. This is because the world position estimation is no longer observable by only the vision SLAM during the indoor flight because the vision scale drifts over time.

**Fig. 11.** The MSF estimated position without the smoothing offset (a and b), and with the proposed smoothing offset algorithm (c and d).

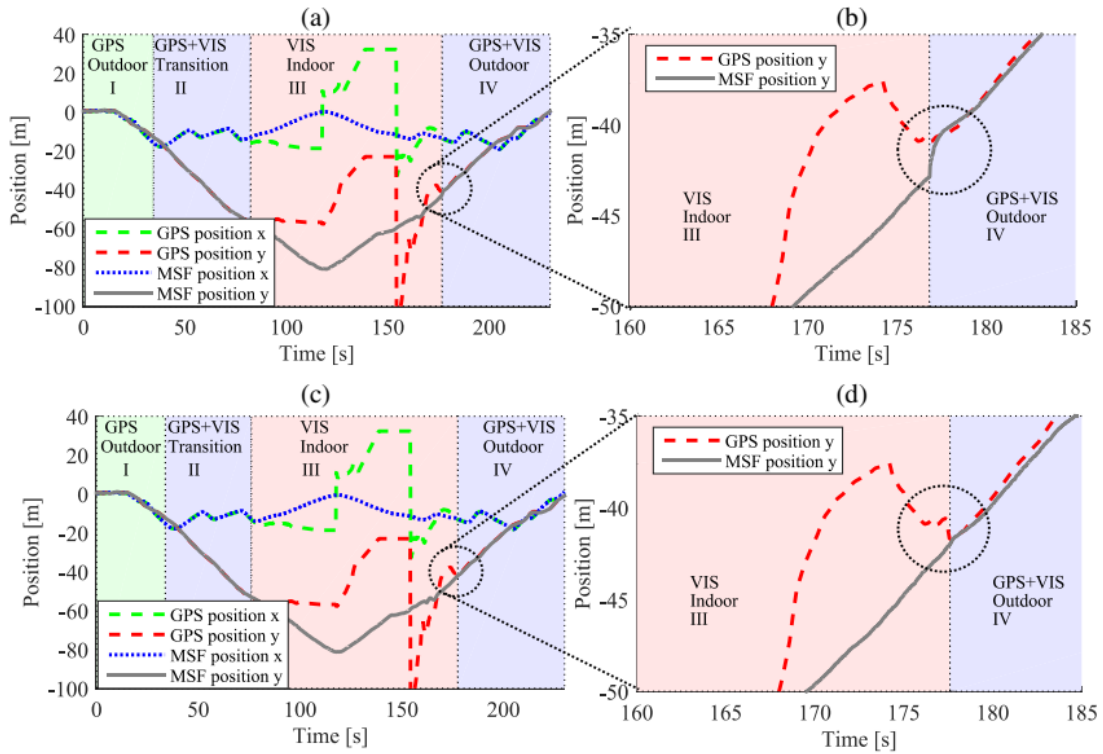
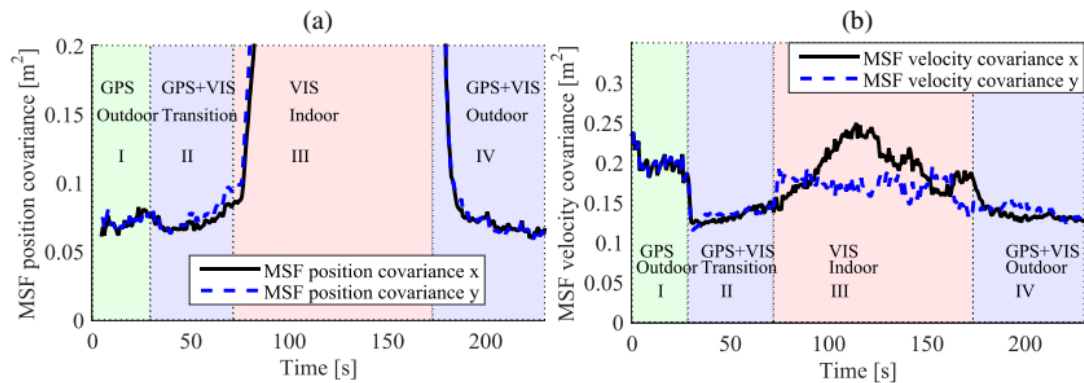


**Fig. 12.** MSF estimated (a) position covariance and (b) velocity covariance.



However, for the velocity covariance, the velocity estimated by the optical flow bounds the covariance to a certain value even without the GPS measurement.

Before going indoors, the GPS and optical flow measurements are used for localization. However, once the UAV is indoors there is no ground truth to validate the UAV position estimation. The estimated flight and estimated GPS paths are thus overlaid on a satellite map, as shown in Fig. 13. The features of ORB\_SLAM2 are shown as color points. The red line is the

Fig. 13. The testing ground and (a) flight trajectories (b) in the flight environment.

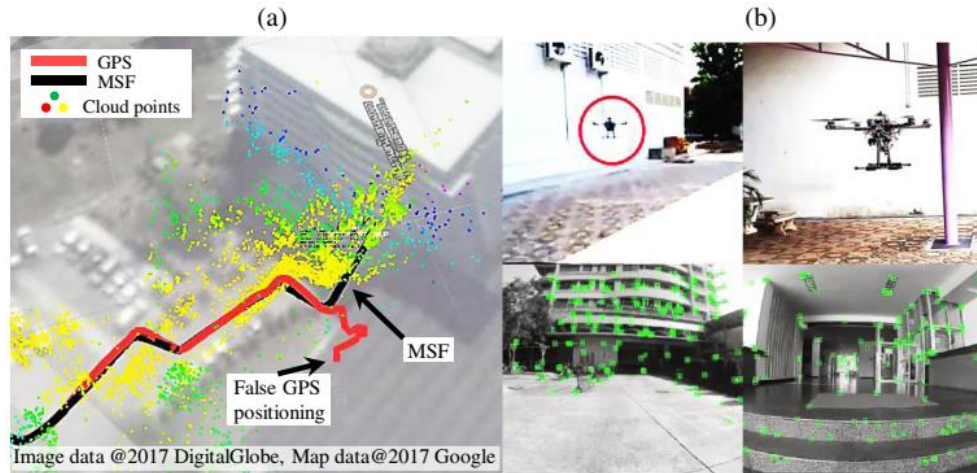
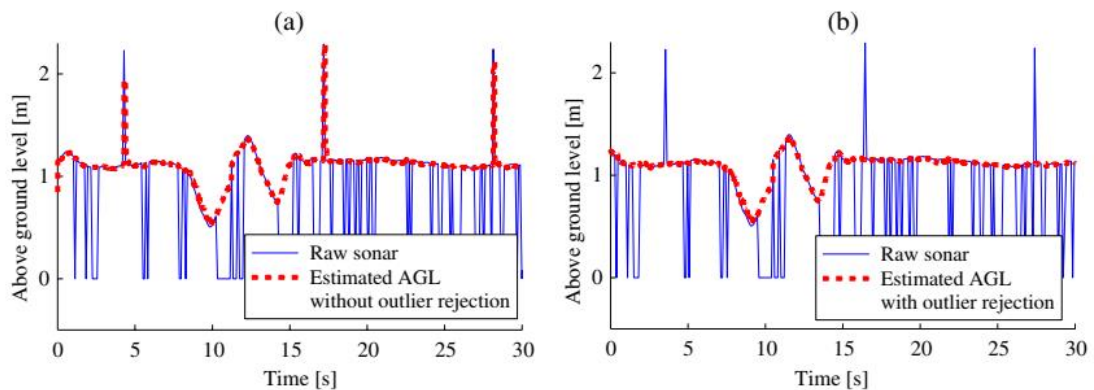


Fig. 14. Above-ground level (AGL) estimated from  $h = p_z - tz$  (a) without outlier rejection and (b) with outlier rejection using Mahalanobis distance check.



GPS signal that has fault value near buildings, and the black line is the position estimated from the MSF. Figure 13b shows the tested UAV and the captured picture from the camera on the UAV at positions outdoors (left) and indoors (right). Video of the experiment can be accessed at <https://goo.gl/1jeK9X> and <https://goo.gl/SDGVDC>.

The estimated terrain data can be validated with the AGL ( $h$ ) measurement as discussed in Sect. 2.2.5. The estimated AGL results and sonar measurements are shown in Fig. 14. Results show that the outlier data could be rejected using Mahalanobis distance method to ensure that optical flow measurement would be properly scaled even when the UAV operates over rougher terrain.

Scale initialization is started as soon as the original ORB\_SLAM2 system is initialized in parallel thread. Result of the scale optimization is shown in Fig. 15. The accelerometer and gyroscope biases converge to steady values after 20 s (Figs. 15a and 15b). The scale initialization takes 30 s to make sure that all variables have already converged (Fig. 15c). Then, scaled vision measurement is processed by smoothing the offset, after that the scaled vision measurement would be available as a measurement for MSF to compute UAV state estimation.

**Fig. 15.** Vision pre-scale process that includes accelerometer and gyroscope biases.

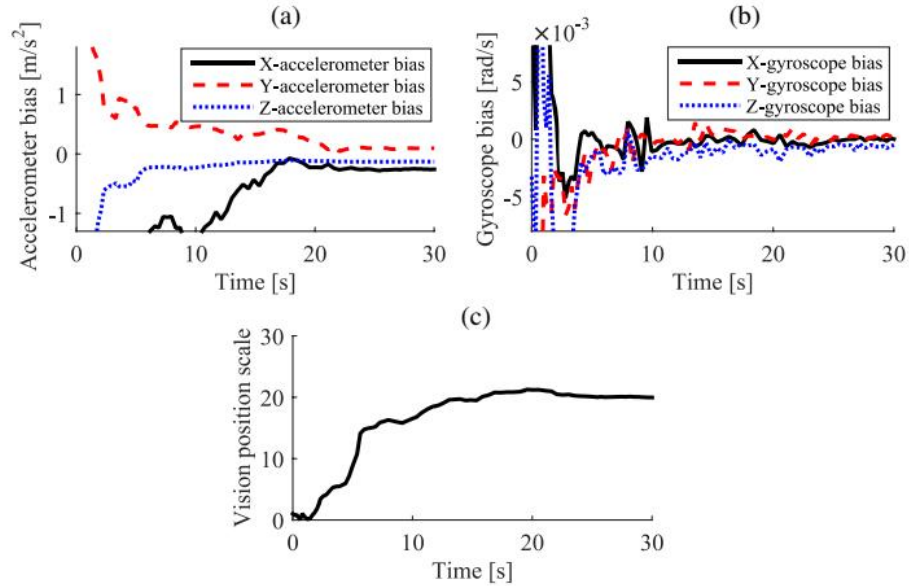
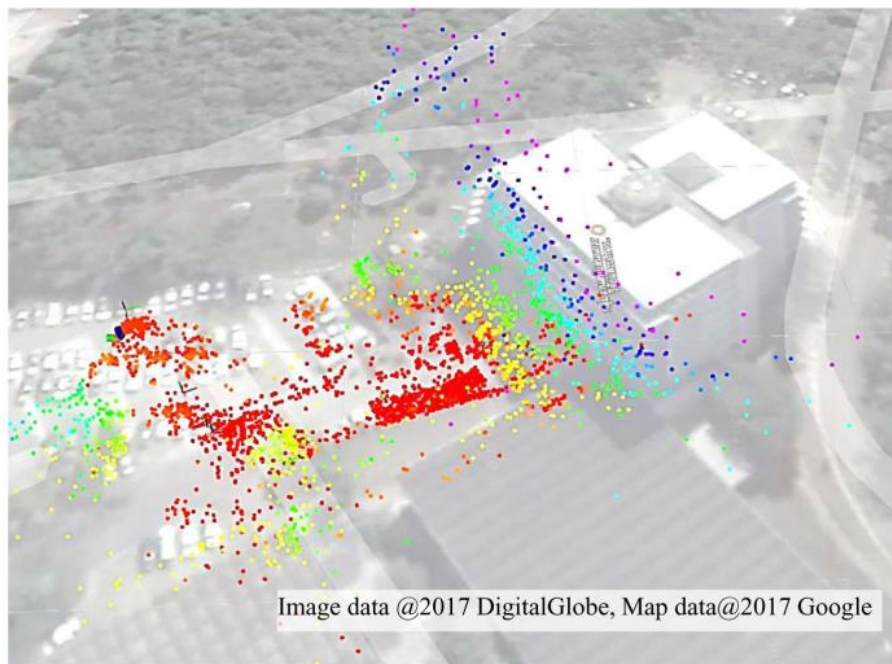


**Fig. 16.** 2D satellite Google map overlay on 3D cloud points from the modified ORB\_SLAM2 algorithm.



The vision scale  $\hat{\lambda}$  and vision position offset  $\hat{\mathbf{p}}_{wv}$  between the vision frame and world frame can be estimated using MSF, and can be used to refine the point cloud outputs from ORB\_SLAM2. All points are adjusted and refined with state estimation during the flight. Figure 16 shows the construction of the estimated cloud point overlays near the building located on a satellite map.

When the UAV is near the building the GPS variance increases, and GPS measurement is then switched off by the GPS quality indicator algorithm as discussed in Sect. 3. Vision, optical flow, and IMU measurements are used in Stage III as shown in Fig. 12. The plots also show that GPS measurement is much influential at this stage. When the UAV is outdoors, the GPS quality factor indicates the GPS measurement is up, then position estimation is adjusted by smoothing the offset before feeding to the MSF for the outdoor state estimation.

## 8. Conclusion

Multi-sensor fusion (MSF) algorithm along with a GPS quality indicator for indoor–outdoor transition and pre-scale vision handling have been proposed in this work. Experiments have shown that the UAV states could be optimized by the proposed measurement method, resulting in a smoother transition when the GPS measurement is lost, or recovered. In field test, the UAV with low-cost sensors could better perform smooth flights from outdoor to indoor environments, and back to outdoor than the conventional method. This indicates that the proposed algorithm is practical and sufficient to operate without high-quality measurement sensors.

In the future, this MSF work may be further improved by adding on more sensor measurements to assist UAV state estimation in more complex tasks, such as avoidance of other moving objects.

## Acknowledgements

The authors would like to thank the smart mechatronics research laboratory for financial support and Intel Cooperation (Thailand) for provision of an Intel NUC computer. In addition, the authors would like to thank Wiwat Sutiwipakorn for commenting on the manuscript.

## References

- Abeywardena, D., Wang, Z., Dissanayake, G., Waslander, S.L., and Kodagoda, S. 2014. Model-aided state estimation for quadrotor micro air vehicles amidst wind disturbances. *In* 2014 IEEE/RSJ International Conference on Intelligent Robots and Systems, Chicago, Ill., USA, 14–18 September 2014. IEEE. pp. 4813–4818. doi: [10.1109/IROS.2014.6943246](https://doi.org/10.1109/IROS.2014.6943246).
- ArduPilot Open Source Autopilot. Available from <http://ardupilot.org/> [accessed 3 August 2017].
- Bloesch, M., Omari, S., Hutter, M., and Siegwart, R. 2015. Robust visual inertial odometry using a direct EKF-based approach. *In* 2015 IEEE/RSJ International Conference on Intelligent Robots and Systems (IROS), Hamburg, Germany, 28 September–2 October 2015. IEEE. pp. 298–304. Available from <http://ieeexplore.ieee.org/abstract/document/7353389/> [accessed 28 July 2017].
- Burri, M., Dätwiler, M., Achtelik, M.W., and Siegwart, R. 2015. Robust state estimation for micro aerial vehicles based on system dynamics. *In* 2015 IEEE International Conference on Robotics and Automation (ICRA), Seattle, Wash., USA, 26–30 May 2015. IEEE. pp. 5278–5283. Available from <http://ieeexplore.ieee.org/abstract/document/7139935/> [accessed 28 July 2017].
- Chowdhary, G., Johnson, E.N., Magree, D., Wu, A., and Shein, A. 2013. GPS-denied indoor and outdoor monocular vision aided navigation and control of unmanned aircraft. *J. Field Robot.* **30**(3): 415–438. doi: [10.1002/rob.21454](https://doi.org/10.1002/rob.21454).
- Crassidis, J.L., Markley, F.L., and Cheng, Y. 2007. Survey of nonlinear attitude estimation methods. *J. Guid. Control Dyn.* **30**(1): 12–28. doi: [10.2514/1.22452](https://doi.org/10.2514/1.22452).
- Dronecrew. 2017. px4tools: PX4 flight analysis tools. Available from <https://github.com/dronecrew/px4tools> [accessed 17 November 2017].
- Engel, J., Schöps, T., and Cremers, D. 2014a. LSD-SLAM: Large-scale direct monocular SLAM. *In* Computer Vision — ECCV 2014. Vol. 8690. Edited by D. Fleet, T. Pajdla, B. Schiele, and T. Tuytelaars. Springer International Publishing, Cham, Switzerland. pp. 834–849. doi: [10.1007/978-3-319-10605-2\\_54](https://doi.org/10.1007/978-3-319-10605-2_54). Available from [http://link.springer.com/10.1007/978-3-319-10605-2\\_54](http://link.springer.com/10.1007/978-3-319-10605-2_54) [accessed 28 July 2017].
- Engel, J., Sturm, J., and Cremers, D. 2014b. Scale-aware navigation of a low-cost quadcopter with a monocular camera. *Rob. Auton. Syst.* **62**(11): 1646–1656. doi: [10.1016/j.robot.2014.03.012](https://doi.org/10.1016/j.robot.2014.03.012).
- Engel, J., Koltun, V., and Cremers, D. 2016. Direct sparse odometry. arXiv preprint arXiv:1607.02565v2. Available from <https://arxiv.org/abs/1607.02565> [accessed 14 November 2017].
- Forster, C., Pizzoli, M., and Scaramuzza, D. 2014. SVO: Fast semi-direct monocular visual odometry. *In* 2014 IEEE International Conference on Robotics and Automation (ICRA), Hong Kong, China, 31 May–7 June 2014. IEEE. pp. 15–22. Available from <http://ieeexplore.ieee.org/abstract/document/6906584/> [accessed 28 July 2017].

- Forster, C., Carlone, L., Dellaert, F., and Scaramuzza, D. 2017. On-manifold preintegration for real-time visual-inertial odometry. *IEEE Trans. Robot.* **33**(1): 1–21. doi: [10.1109/TRO.2016.2597321](https://doi.org/10.1109/TRO.2016.2597321).
- Hutchison, D., Kanade, T., Kittler, J., Kleinberg, J.M., Mattern, F., Mitchell, J.C., and Schiele, B. 2010. Monocular 3D scene modeling and inference: Understanding multi-object traffic scenes. In *Computer Vision — ECCV 2010*. Vol. 6314. Edited by K. Daniilidis, P. Maragos, and N. Paragios. Springer Berlin Heidelberg, Berlin, Heidelberg, Germany. pp. 467–481. doi: [10.1007/978-3-642-15561-1\\_34](https://doi.org/10.1007/978-3-642-15561-1_34). Available from [http://link.springer.com/10.1007/978-3-642-15561-1\\_34](http://link.springer.com/10.1007/978-3-642-15561-1_34) [accessed 28 July 2017].
- Kamel, M., Stastny, T., Alexis, K., and Siegwart, R. 2017. Model predictive control for trajectory tracking of unmanned aerial vehicles using robot operating system. In *Robot operating system (ROS)*. Edited by A. Koubaa. Springer, Cham, Switzerland. pp. 3–39. Available from [http://link.springer.com/chapter/10.1007/978-3-319-54927-9\\_1](http://link.springer.com/chapter/10.1007/978-3-319-54927-9_1) [accessed 28 July 2017].
- Kealy, A., Roberts, G., and Retscher, G. 2010. Evaluating the performance of low cost MEMS inertial sensors for seamless indoor/outdoor navigation. In 2010 IEEE/ION Position, Location and Navigation Symposium (PLANS), Indian Wells, Calif., USA, 4–6 May 2010. IEEE. pp. 157–167. Available from <http://ieeexplore.ieee.org/abstract/document/5507132/> [accessed 28 July 2017].
- Leishman, R.C., and McLain, T.W. 2015. Multiplicative extended Kalman filter for relative rotorcraft navigation. *J. Aerosp. Inf. Syst.* **12**(12): 728–744. doi: [10.2514/1.1010236](https://doi.org/10.2514/1.1010236).
- Lynen, S., Achtelik, M.W., Weiss, S., Chli, M., and Siegwart, R. 2013. A robust and modular multi-sensor fusion approach applied to MAV navigation. In 2013 IEEE/RSJ International Conference on Intelligent Robots and Systems (IROS), Tokyo, Japan, 3–7 November 2013. IEEE. pp. 3923–3929. Available from <http://ieeexplore.ieee.org/abstract/document/6696917/> [accessed 28 July 2017].
- Maye, J., Furgale, P., and Siegwart, R. 2013. Self-supervised calibration for robotic systems. In 2013 IEEE Intelligent Vehicles Symposium (IV), Gold Coast, QLD, Australia, 23–26 June 2013. IEEE. pp. 473–480. doi: [10.1109/IVS.2013.6629513](https://doi.org/10.1109/IVS.2013.6629513).
- Meier, L., Tanskanen, P., Heng, L., Lee, G.H., Fraundorfer, F., and Pollefeys, M. 2012. PIXHAWK: A micro aerial vehicle design for autonomous flight using onboard computer vision. *Auton. Robots*, **33**(1–2): 21–39. doi: [10.1007/s10514-012-9281-4](https://doi.org/10.1007/s10514-012-9281-4).
- Meier, L., Camacho, J., Godbolt, B., Goppert, J., Heng, L., and Lizarraga, M. 2013. MAVLink: Micro air vehicle communication protocol. Available from <http://qgroundcontrol.org/mavlink/start> [accessed 26 November 2017].
- Meier, L., Honegger, D., and Pollefeys, M. 2015. PX4: A node-based multithreaded open source robotics framework for deeply embedded platforms. In 2015 IEEE International Conference on Robotics and Automation (ICRA), Seattle, Wash., USA, 26–30 May 2015. IEEE. pp. 6235–6240. Available from <http://ieeexplore.ieee.org/abstract/document/7140074/> [accessed 28 July 2017].
- Mur-Artal, R., and Tardós, J.D. 2017. Visual-inertial monocular SLAM with map reuse. *IEEE Robot. Autom. Lett.* **2**(2): 796–803. doi: [10.1109/LRA.2017.2653359](https://doi.org/10.1109/LRA.2017.2653359).
- Nyholm, P.W. 2015. Globally consistent map generation in GPS-degraded environments. Available from <http://scholarsarchive.byu.edu/etd/5262/> [accessed 28 July 2017].
- Sa, I., Kamel, M., Khanna, R., Popovic, M., Nieto, J., and Siegwart, R. 2017. Dynamic system identification, and control for a cost effective open-source VTOL MAV. arXiv preprint arXiv:1701.08623. Available from <https://arxiv.org/abs/1701.08623> [accessed 28 July 2017].
- Santamaria-Navarro, A., Sola, J., and Andrade-Cetto, J. 2015. High-frequency MAV state estimation using low-cost inertial and optical flow measurement units. In 2015 IEEE/RSJ International Conference on Intelligent Robots and Systems (IROS), Hamburg, Germany, 28 September–2 October 2015. IEEE. pp. 1864–1871. Available from <http://ieeexplore.ieee.org/abstract/document/7353621/> [accessed 28 July 2017].
- Serrano, D., de Haag, M.U., Dill, E., Vilardaga, S., and Duan, P. 2014. Seamless indoor-outdoor navigation for unmanned multi-sensor aerial platforms. *Int. Arch. Photogramm. Remote Sens. Spatial Inf. Sci.* **XL-3/W1**(3): 115–122. doi: [10.5194/isprsarchives-XL-3-W1-115-2014](https://doi.org/10.5194/isprsarchives-XL-3-W1-115-2014).
- Shen, S., Mulgaonkar, Y., Michael, N., and Kumar, V. 2014. Multi-sensor fusion for robust autonomous flight in indoor and outdoor environments with a rotorcraft MAV. In 2014 IEEE International Conference on Robotics and Automation (ICRA), Hong Kong, China, 31 May–7 June 2014. IEEE. pp. 4974–4981. Available from <http://ieeexplore.ieee.org/abstract/document/6907588/> [accessed 28 July 2017].
- Shi, J., and Cannon, M.E. 1995. Critical error effects and analysis in carrier phase-based airborne GPS positioning over large areas. *Bull. Géod.* **69**(4): 261–273. doi: [10.1007/BF00806738](https://doi.org/10.1007/BF00806738).
- Sola, J. 2015. Quaternion kinematics for the error-state Kalman filter. Available from <https://hal.archives-ouvertes.fr/hal-01122406/document> [accessed 28 July 2017].
- Weiss, S.M. 2012. Vision based navigation for micro helicopters. Doctoral thesis, ETH Zurich, Zürich, Switzerland. doi: [10.3929/ethz-a-007344020](https://doi.org/10.3929/ethz-a-007344020). Available from <https://www.research-collection.ethz.ch/handle/20.500.11850/52698> [accessed 14 November 2017].
- Weiss, S.M., Scaramuzza, D., and Siegwart, R. 2011. Monocular-SLAM-based navigation for autonomous micro helicopters in GPS-denied environments. *J. Field Robot.* **28**(6): 854–874. doi: [10.1002/rob.20412](https://doi.org/10.1002/rob.20412).
- Yang, Z., and Shen, S. 2017. Monocular visual-inertial state estimation with online initialization and camera-IMU extrinsic calibration. *IEEE Trans. Autom. Sci. Eng.* **14**(1): 39–51. doi: [10.1109/TASE.2016.2550621](https://doi.org/10.1109/TASE.2016.2550621).

## VITAE

**Name**                      Thanabadee Bulunseechart

**Student ID**                5710120027

### **Educational Attainment**

Degree	Name of Institution	Year of Graduation
Bachelor of Engineering in Mechatronic Engineering	Prince of Songkla University	2012

### **Scholarship Awards during Enrolment**

1. Engineering Graduate scholarship, 2014.
2. Graduate School Dissertation Funding for Thesis, 2015.

### **List of Publication and Proceeding**

#### **1. Publication of conference paper presented in Chapter 2:**

Thanabadee Bulunseechart and Pruittikorn Smithmaitrie, Comparison of state estimation algorithms for autonomous GPS-Inertial navigation for UAV application, *The 8th PSU-UNS International Conference on Engineering and Technology (ICET-2017)*, June 8-10, 2017, Novi Sad, Serbia.

#### **2. Publication of journal article presented in Chapter 3:**

Thanabadee Bulunseechart, and Pruittikorn Smithmaitrie 2018 A Method for UAV Multi-Sensor Fusion 3D-Localization under Degraded or Denied GPS Situation. *Journal of Unmanned Vehicle Systems*. 6(3): 155-176. doi:10.1139/juvs-2018-0007